

Searching for Signs of the Second Higgs Doublet

Nathaniel Craig,^{a,b} Jamison Galloway,^c Scott Thomas^a

^a*Department of Physics, Rutgers University
Piscataway, NJ 08854*

^b*School of Natural Sciences, Institute for Advanced Study
Princeton, NJ 08540*

^c*Dipartimento di Fisica, Università di Roma “La Sapienza” and INFN Sezione di Roma
I-00185 Rome, Italy*

E-mail: ncraig@ias.edu, jamison.galloway@roma1.infn.it,
scthomas@physics.rutgers.edu

ABSTRACT: The search for evidence of extended electroweak symmetry breaking has entered a new phase with the discovery of a Standard Model (SM)-like Higgs at the LHC. The measurement of Higgs couplings and direct searches for additional scalars provide complementary avenues for the discovery of new degrees of freedom. This complementarity is particularly sharp in two Higgs doublet models (2HDMs) where the couplings of the SM-like Higgs may be directly related to the LHC signals of additional scalars. In this work we develop a strategy for searching for the second Higgs doublet given the LHC signals of the recently discovered SM-like Higgs. We focus on a motivated parameter space of flavor- and CP-conserving 2HDMs in which the couplings of all scalars to SM states are controlled by two parameters. We construct fits in this parameter space to the signals of the SM-like Higgs and translate these fits into signal expectations for future measurements of both the SM-like Higgs and additional scalars, identifying the most promising search channels for discovery or exclusion of new physics. When kinematically accessible, decays of the heavy neutral scalar Higgs to two light Higgs scalars, $H \rightarrow hh$, and decays of the pseudoscalar Higgs to a light Higgs scalar and Z boson, $A \rightarrow Zh$, provide promising avenues for discovery even when the couplings of the light Higgs are within a few percent of SM predictions. When the couplings of the light Higgs are exceptionally close to those of the SM, decays of heavier neutral scalars to $\gamma\gamma$ and $\tau^+\tau^-$ become particularly important for discovery.

Contents

1	Introduction	2
2	The Second Higgs Doublet	5
2.1	Decays to the SM-like Higgs	8
3	Couplings of the SM-like Higgs	10
4	Signals of the Second Higgs Doublet	15
5	Signs of the Second Higgs Doublet in the SM-like Higgs Couplings	17
5.1	Inclusive production of h with $h \rightarrow \tau^+\tau^-$ or $h \rightarrow \mu^+\mu^-$	18
5.2	Vh /VBF production of h with $h \rightarrow \tau^+\tau^-$	18
5.3	Vh production of h with $h \rightarrow b\bar{b}$	20
5.4	Vh /VBF production of h with $h \rightarrow \gamma\gamma$	21
5.5	Vh /VBF production of h with $h \rightarrow VV^*$	21
5.6	$t\bar{t}$ associated production of h with $h \rightarrow \gamma\gamma$	21
5.7	Inclusive production of h with $h \rightarrow Z\gamma$	22
5.8	Future prospects	22
6	Direct Signs of the Second Higgs Doublet	23
6.1	Inclusive production of H with $H \rightarrow VV^{(*)}$	29
6.2	Inclusive production of H with $H \rightarrow \gamma\gamma$	30
6.3	Inclusive production of A with $A \rightarrow \gamma\gamma$	31
6.4	Inclusive production of H or A with $H, A \rightarrow \tau^+\tau^-$ or $H, A \rightarrow \mu^+\mu^-$	33
6.5	Inclusive production with $H \rightarrow hh$	34
6.6	Inclusive production with $A \rightarrow Zh$	35
6.7	$t\bar{t}$ production with $t \rightarrow H^\pm\bar{b}$ and $H^\pm \rightarrow \tau^\pm\nu$	36
6.8	Signals of degenerate Higgses	37
7	Conclusions	39
A	Hhh Coupling	40
B	Standard-Model Like Higgs Fit Data	42

1 Introduction

The discovery of a Higgs-like boson at the LHC [1, 2] provides an unprecedented opportunity in the search for physics beyond the Standard Model (BSM). Any significant deviations from SM predictions for Higgs couplings would provide an immediate indication of new physics, while the Higgs may also serve as a portal into an extended electroweak symmetry breaking (EWSB) sector with additional scalar degrees of freedom. These two possibilities are closely related, as mixing among scalars in an extended EWSB sector leads to deviations from Standard Model Higgs couplings. Given the discovery of one Higgs boson, the search for additional Higgs scalars is a crucial objective for current and future searches at the LHC.

There are three principal avenues to searching for a second Higgs. The first is to study the couplings of the SM-like Higgs h itself, as the couplings of h are altered from their Standard Model values by mixing between scalars. The second is to search for new states in SM Higgs channels [3], since additional scalars share many of the same production and decay modes as the SM-like Higgs. The third is to search for new states in additional channels, such as those in which heavier scalars decay to final states involving the SM-like Higgs [4]. There is extensive interplay between these three avenues, since the couplings of the SM-like Higgs are correlated with the variation in production and decay modes of additional scalars. Indeed, many types of extended EWSB sectors are already tightly constrained by measurements of the SM-like Higgs couplings alone.

In order to optimally exploit the interplay between these search channels, it is instrumental to develop a map between the couplings of the observed SM-like Higgs and the couplings of additional Higgs scalars. Typically this map depends on the details of the extended EWSB sector. In this work we will focus on EWSB sectors whose low-energy effective theory is described by two Higgs doublets [5–8]. Theories with two Higgs doublets provide a motivated parameter space for probing extended electroweak symmetry breaking. Additional Higgs doublets arise in many models of natural BSM physics, including the minimal supersymmetric extension of the SM [9], twin Higgs models [10], and certain composite Higgs models [11]. More generally, two Higgs doublet models (2HDMs) provide a simple parameterization of extensions of the Higgs sector that captures the most important features; other extended EWSB sectors are qualitatively similar.

In this paper we classify the correlations between search channels, focusing on the most important production and decay topologies for the discovery of additional states. Two Higgs doublet models exhibit a vast signal space involving the five physical scalar particles that remain after EWSB: two neutral CP-even scalars, h , H ; one neutral CP-odd pseudoscalar, A ; and two charged scalars, H^+ and H^- . The parameter space of these 2HDMs can accommodate a wide range of variations in the production and decay modes of the SM-like Higgs boson, as well as discoverable rates for the production and decay of additional scalars [4, 12–17].¹ Although the available parameter space of completely general 2HDMs is quite broad, there is

¹For reviews of 2HDM phenomenology, see [18, 19]. For recent work on 2HDM at the LHC in light of the Higgs discovery, see e.g. [3, 4, 20–33].

a strongly motivated subspace that provides a predictive map between the couplings of the SM-like Higgs and the potential signals of additional scalars. In particular, tight constraints on flavor-changing neutral currents disfavor 2HDM with tree-level flavor violation. Such prohibitive flavor violation may be avoided by four discrete choices of tree-level Yukawa couplings between the Higgs doublets and SM fermions. Similarly, limits on additional sources of CP violation favor 2HDM with a CP-conserving potential. The avoidance of tree-level FCNCs and explicit CP violation limits the available parametric freedom to the extent that the couplings of all states to SM fermions and gauge bosons may be described solely in terms of two mixing angles.²

Within this framework, we will study the interplay between current fits to the SM-like Higgs couplings driven by LHC data and the range of couplings available to additional scalars. For definiteness, we focus on the scenario in which the observed SM-like Higgs is the lightest CP-even neutral scalar h , although the alternate case remains interesting. First, we construct fits to current Higgs signals at the LHC and Tevatron in terms of the 2HDM parameter space following the approach of [3, 34]. At present these fits have the greatest impact on the 2HDM parameter space among current measurements. We find all four discrete 2HDM types are constrained to lie close to the alignment limit where the couplings of h are SM-like. Two of these types (Type 2 and Type 4) must lie particularly close to the alignment limit, with the coupling of the SM-like Higgs to vector bosons constrained to lie within 10% of the Standard Model value at 95% CL over the entire parameter space.

Given the constraints imposed by the coupling fits of the SM-like Higgs, we identify the most promising search channels for discovering additional scalars at the LHC. There is a natural ordering of these channels when the additional scalars are similar in mass, as is expected to be the case when the observed CP-even Higgs is mostly SM-like. In this case the kinematically available decay modes include the usual decays to SM gauge bosons and fermions, as well as decays involving one or more SM-like Higgs bosons. For example, the heavy CP-even Higgs may decay to two light CP-even Higgses, $H \rightarrow hh$; the CP-odd pseudoscalar Higgs may decay to a light CP-even Higgs and a Z boson, $A \rightarrow Zh$; and the charged Higgses H^\pm may decay to an SM-like Higgs and a W^\pm boson, $H^\pm \rightarrow W^\pm h$. These modes are often complementary to direct decays to SM final states.

The consistency of Higgs coupling fits with SM predictions suggests that the 2HDM Higgs sector is close to the alignment limit where the couplings of one CP-even Higgs scalar are SM-like. As illustrated in Table 1, in the exact alignment limit certain decay modes of heavy scalars vanish, including $H \rightarrow VV$, $H \rightarrow hh$, and $A \rightarrow Zh$. However, even when close to the alignment limit, these modes may still dominate the decay products of the heavy scalars if they are kinematically accessible. This is particularly likely when $m_H, m_A < 2m_t$, in which case the decays $H \rightarrow VV$, $H \rightarrow hh$, and $A \rightarrow Zh$ only compete with decays into bottom

²Note that even if tree-level flavor violation is forbidden, significant flavor violation may still arise at one loop and contribute to precision flavor observables such as $B \rightarrow X_s \gamma$. In this work we will not consider additional constraints coming from precision flavor measurements, since loop-induced contributions to these processes from additional Higgs scalars may be reduced by destructive interference.

Second Higgs Doublet Decay Topology	Alignment Limit
$H \rightarrow WW, ZZ$	–
$H, A \rightarrow \gamma\gamma$	✓
$H, A \rightarrow \tau\tau, \mu\mu$	✓
$H, A \rightarrow tt$	✓
$A \rightarrow Zh$	–
$H \rightarrow hh$	–
$t \rightarrow H^\pm b$	✓

Table 1. Leading 2HDM decay topologies with unsuppressed production cross sections near the alignment limit for neutral scalars with mass spectra $m_H \sim m_A > 2m_h$, and top quark with $m_{H^\pm} < m_t + m_b$. A checkmark (dash) indicates that the partial decay width approaches a constant (vanishes) in the $\cos(\beta - \alpha) = 0$ alignment limit. The first five topologies give additional non-Standard Model contributions to Standard Model Higgs search channels. The remaining topologies are specific Second Higgs Doublet search channels. Altogether these topologies form a basis for Second Higgs Doublet searches with non-SM-like boson masses greater than the SM-like Higgs boson.

quarks. If the partial widths for $H \rightarrow VV$, $H \rightarrow hh$, and $A \rightarrow Zh$ exceed the partial widths for decays into fermions, the resulting branching ratios only weakly depend on proximity to the alignment limit. However, proximity to the alignment limit *does* imply that associated production modes for H involving vector couplings – such as vector boson fusion or production in association with a W or Z boson – are likely to be suppressed. Thus the production of both H and the pseudoscalar A are likely to be dominated by gluon fusion, in which case discovering H and A at the LHC requires focusing on distinctive final states.

The most promising final states for the discovery of additional Higgs scalars change as the couplings are varied. For the heavy neutral Higgs H , the decays to hh, VV and $\gamma\gamma, \tau^+\tau^-$ play complementary roles depending on proximity to the alignment limit. When kinematically available, the decay of $H \rightarrow hh$ is significant even for small deviations from the alignment limit; it dominates the decay products of H for $2m_h < m_H < 2m_t$ and may continue to dominate even when $m_H > 2m_t$. However, this partial width falls as the alignment limit is approached, much like the rate for H to decay into two vectors. This alone does not guarantee that the branching ratio is small, since $\Gamma(H \rightarrow hh) \propto m_H^3/v^2$ and typically dominates the total width until $g_{HV V}/g_{H_{SM} V V} \lesssim \mathcal{O}(m_b/m_H)$ unless the coupling of H to bottom quarks

is parametrically enhanced. Since the coupling of the SM-like Higgs to vector bosons can be measured at the 14 TeV LHC to only $\mathcal{O}(8\%)$ accuracy with 3000 fb^{-1} of data [42], this suggests that $H \rightarrow hh$ may constitute a substantial fraction of H decays even if asymptotic measurements of Higgs couplings at the LHC remain consistent with SM expectations. Of course, it is also possible that the 2HDM Higgs sector lies very close to the alignment limit. For $g_{HVV}/g_{H_{SM}VV} \lesssim \mathcal{O}(m_b/m_H)$, the branching ratio for $H \rightarrow hh$ is diminished, but at the same time decays to $\gamma\gamma$ and $\tau^+\tau^-$ become increasingly important because they do not decouple in the alignment limit.

The same is true of the pseudoscalar Higgs A with respect to the decays to Zh and $\gamma\gamma, \tau^+\tau^-$, respectively. The partial width $\Gamma(A \rightarrow Zh)$ likewise scales as $\propto m_A^3/v^2$ and vanishes in the alignment limit. Unless the coupling of A to fermions is parametrically enhanced, $A \rightarrow Zh$ often dominates the total width until very close to the alignment limit. In the exact alignment limit, decays to $\gamma\gamma$ and $\tau^+\tau^-$ become important.

Our paper is organized as follows: In Section 2 we discuss the relevant aspects of 2HDMs, focusing on the alignment limit in which one CP-even neutral scalar is approximately SM-like, and define the restricted parameter space used in our study. In Section 3 we construct fits to the couplings of the SM-like Higgs in the context of various 2HDM types, using all available data from the LHC and Tevatron. In Section 4 we present our procedure for parameterizing the production cross sections and branching ratios of the additional Higgs scalars. We use the coupling fits in Section 5 to explore the range of signals available in future measurements of the SM-like Higgs in production and decay modes that are currently poorly constrained. In Section 6 we use the coupling fits to the SM-like Higgs to probe the range of signals available to the additional physical Higgs bosons in a 2HDM. We conclude in Section 7 with various suggestions for LHC search strategies motivated by the range of possible 2HDM signals. Details of the 2HDM scalar potential and the Higgs coupling fit procedure are reserved for appendices.

2 The Second Higgs Doublet

The general parameter space of 2HDMs is large, but it can be efficiently reduced using a small set of motivated assumptions. Specifically, in this work we focus on CP conservation in the potential and the absence of tree-level contributions to flavor-changing neutral currents; these are reasonable assumptions since additional sources of CP violation and FCNCs are tightly constrained. Although the mass spectrum of 2HDM is in principle arbitrary, here we wish to focus on a spectrum with two approximate scales: a light SM-like Higgs h at $m_h \sim 126 \text{ GeV}$, and the remaining physical Higgs scalars H, A, H^\pm clustered together at an equal or higher scale with $m_H \sim m_A \sim m_{H^\pm}$. In this case the only available decay modes of the SM-like Higgs are those involving SM states. This allows us to describe the couplings of the SM-like Higgs in terms of two free parameters, and gives a natural ordering for the additional scalar decay modes that are kinematically accessible. With these assumptions, it is straightforward

to map the current fits to the signals of the SM-like Higgs to the production and decay rates of the remaining scalars.³

The absence of tree-level flavor-changing neutral currents in theories with multiple Higgs doublets is guaranteed by the Glashow-Weinberg condition [35] that all fermions of a given representation receive their masses through renormalizable Yukawa couplings to a single Higgs doublet, in which case the tree-level couplings of neutral Higgs bosons are diagonal in the mass eigenbasis. This restriction may be enforced by a discrete symmetry acting on the doublets. In theories with only two Higgs doublets, the Yukawa couplings are

$$V_{yukawa} = - \sum_{i=1,2} \left(Q\tilde{\Phi}_i y_i^u \bar{u} + Q\Phi_i y_i^d \bar{d} + L\Phi_i y_i^e \bar{e} + \text{h.c.} \right) \quad (2.1)$$

and the Glashow-Weinberg condition is satisfied by four discrete assignments, where by convention up-type quarks are always taken to couple to Φ_2 :

- Type 1, in which $y_1^{u,d,e} = 0$; all fermions couple to one doublet.
- Type 2, in which $y_1^u = y_2^d = y_2^e = 0$; the up-type quarks couple to one doublet and the down-type quarks and leptons couple to the other.
- Type 3, in which $y_1^u = y_1^d = y_2^e = 0$; quarks couple to one doublet and leptons to the other.
- Type 4, in which $y_1^u = y_1^e = y_2^d = 0$; up-type quarks and leptons couple to one doublet and down-type quarks couple to the other.

The signals of Type 3 and Type 4 2HDM typically resemble those of Type 1 and Type 2 2HDM, respectively, since these pairings share the same quark assignments and thus the same parametric scaling for dominant production and decay modes.⁴ The primary exception is for signals involving leptonic final states, for which the branching ratios are parametrically enhanced (suppressed) in Type 3 (4) 2HDM compared to their Type 1 (2) counterparts. In what follows we will largely focus on 2HDM of Type 1 and 2, though we will discuss distinctive features of Type 3 and 4 where appropriate.

The most general scalar potential for a CP-conserving 2HDM allowed by gauge invariance is given in Appendix A. Including the vacuum expectation values, there are 12 real degrees of freedom in the potential; 9 remain free after minimizing the potential and fixing the electroweak symmetry breaking $v^2 = v_1^2 + v_2^2 = (246 \text{ GeV})^2$. A convenient basis for the remaining free parameters consists of the ratio of vacuum expectation values of $\Phi_{1,2}^0$, parameterized by

$$\tan \beta \equiv |\langle \Phi_2^0 \rangle / \langle \Phi_1^0 \rangle| ; \quad (2.2)$$

³Note that although we focus on the case where the light CP-even scalar h is the SM-like Higgs, the coupling fits are identical (under $\alpha \rightarrow \alpha + \pi/2$) when the heavy CP-even scalar H is the SM-like Higgs, up to the possible effects of new decay modes involving additional scalars.

⁴Note that some other 2HDM studies switch Type 3 and Type 4 assignments.

the mixing angle α that diagonalizes the 2×2 neutral scalar $h - H$ mass squared matrix,

$$\begin{pmatrix} \sqrt{2} \operatorname{Re}(\Phi_2^0) - v_2 \\ \sqrt{2} \operatorname{Re}(\Phi_1^0) - v_1 \end{pmatrix} = \begin{pmatrix} \cos \alpha & \sin \alpha \\ -\sin \alpha & \cos \alpha \end{pmatrix} \begin{pmatrix} h \\ H \end{pmatrix}; \quad (2.3)$$

the four physical masses m_h, m_H, m_A, m_{H^\pm} ; and the couplings λ_5, λ_6 , and λ_7 , shown explicitly in Appendix A. The discrete symmetry that ensures the Glashow-Weinberg condition also requires $\lambda_6 = \lambda_7 = 0$, though in what follows we will consider the effects of nonzero $\lambda_{6,7}$ where appropriate.

The angles α and β fully determine the couplings between a single physical Higgs boson and two gauge bosons or two fermions, as well as the coupling between two Higgses and a single gauge boson. Only renormalizable couplings involving three and four physical Higgs bosons depend on the additional parameters of the potential. Therefore if we identify the lightest CP-even neutral Higgs scalar h with the observed SM-like Higgs at 126 GeV, with the remaining scalars H, A, H^\pm equal in mass or heavier, then deviations in the production and decay rates of the SM-like Higgs from the SM prediction may be parameterized entirely in terms of α and β .

Thus far, the signals of the Higgs boson measured by ATLAS and CMS have remained largely consistent with SM predictions. This consistency suggests that if the EWSB sector is described by a 2HDM, it is likely to lie near the alignment limit where $\sin(\beta - \alpha) = 1$ and the coupling of h to vector bosons is SM-like [36].⁵ Given this preference, it is useful to express the couplings of various Higgs scalars to SM fermions and gauge bosons in terms of deviations from the alignment limit. In particular, the couplings to fermions in various types of 2HDM depend on four trigonometric functions of α, β that may be expanded near the alignment limit. The couplings of the CP-even scalar h depend entirely on the combinations

$$\sin(\beta - \alpha) - \tan \beta \cos(\beta - \alpha) \simeq 1 - \tan \beta \cos(\beta - \alpha) - \frac{1}{2} \cos^2(\beta - \alpha) + \mathcal{O}(\cos^4(\beta - \alpha)) \quad (2.4)$$

$$\sin(\beta - \alpha) + \cot \beta \cos(\beta - \alpha) \simeq 1 + \cot \beta \cos(\beta - \alpha) - \frac{1}{2} \cos^2(\beta - \alpha) + \mathcal{O}(\cos^4(\beta - \alpha)) \quad (2.5)$$

while the couplings of the remaining scalars depend on the combinations

$$\tan \beta \sin(\beta - \alpha) + \cos(\beta - \alpha) \simeq \tan \beta \left[1 + \cot \beta \cos(\beta - \alpha) - \frac{1}{2} \cos^2(\beta - \alpha) + \mathcal{O}(\cos^4(\beta - \alpha)) \right] \quad (2.6)$$

$$\cot \beta \sin(\beta - \alpha) - \cos(\beta - \alpha) \simeq \cot \beta \left[1 - \tan \beta \cos(\beta - \alpha) - \frac{1}{2} \cos^2(\beta - \alpha) + \mathcal{O}(\cos^4(\beta - \alpha)) \right] \quad (2.7)$$

In the second equality we have expanded around $\sin(\beta - \alpha) = 1$. In Table 2 we use these trigonometric identities to express the fermion and vector couplings of all scalars in the four discrete types of flavor-preserving 2HDM as a function of $\tan \beta$ and $\beta - \alpha$.

⁵Note that we distinguish the alignment limit $\sin(\beta - \alpha) = 1$ from the decoupling limit $m_A^2 \gg |\lambda_i|v^2$. When $m_{H,A,H^\pm} \gg m_h$ these limits coincide, but in general we also wish to consider the case where all scalars are relatively light but the couplings of h are entirely SM-like, perhaps due to accidental cancellations in the 2HDM potential.

$y_{2\text{HDM}}/y_{\text{SM}}$	2HDM 1	2HDM 2	2HDM 3	2HDM 4
hVV	$s_{\beta-\alpha}$	$s_{\beta-\alpha}$	$s_{\beta-\alpha}$	$s_{\beta-\alpha}$
hQu	$s_{\beta-\alpha} + c_{\beta-\alpha}/t_\beta$	$s_{\beta-\alpha} + c_{\beta-\alpha}/t_\beta$	$s_{\beta-\alpha} + c_{\beta-\alpha}/t_\beta$	$s_{\beta-\alpha} + c_{\beta-\alpha}/t_\beta$
hQd	$s_{\beta-\alpha} + c_{\beta-\alpha}/t_\beta$	$s_{\beta-\alpha} - t_\beta c_{\beta-\alpha}$	$s_{\beta-\alpha} + c_{\beta-\alpha}/t_\beta$	$s_{\beta-\alpha} - t_\beta c_{\beta-\alpha}$
hLe	$s_{\beta-\alpha} + c_{\beta-\alpha}/t_\beta$	$s_{\beta-\alpha} - t_\beta c_{\beta-\alpha}$	$s_{\beta-\alpha} - t_\beta c_{\beta-\alpha}$	$s_{\beta-\alpha} + c_{\beta-\alpha}/t_\beta$
HVV	$c_{\beta-\alpha}$	$c_{\beta-\alpha}$	$c_{\beta-\alpha}$	$c_{\beta-\alpha}$
HQu	$c_{\beta-\alpha} - s_{\beta-\alpha}/t_\beta$	$c_{\beta-\alpha} - s_{\beta-\alpha}/t_\beta$	$c_{\beta-\alpha} - s_{\beta-\alpha}/t_\beta$	$c_{\beta-\alpha} - s_{\beta-\alpha}/t_\beta$
HQd	$c_{\beta-\alpha} - s_{\beta-\alpha}/t_\beta$	$c_{\beta-\alpha} + t_\beta s_{\beta-\alpha}$	$c_{\beta-\alpha} - s_{\beta-\alpha}/t_\beta$	$c_{\beta-\alpha} + t_\beta s_{\beta-\alpha}$
HLe	$c_{\beta-\alpha} - s_{\beta-\alpha}/t_\beta$	$c_{\beta-\alpha} + t_\beta s_{\beta-\alpha}$	$c_{\beta-\alpha} + t_\beta s_{\beta-\alpha}$	$c_{\beta-\alpha} - s_{\beta-\alpha}/t_\beta$
AVV	0	0	0	0
AQu	$1/t_\beta$	$1/t_\beta$	$1/t_\beta$	$1/t_\beta$
AQd	$-1/t_\beta$	t_β	$-1/t_\beta$	t_β
ALe	$-1/t_\beta$	t_β	t_β	$-1/t_\beta$

Table 2. The tree-level couplings of the neutral Higgs bosons h, H , and A to up- and down-type quarks, leptons, and massive gauge bosons relative to the SM Higgs boson couplings as functions of α and β in the four types of 2HDM models satisfying the Glashow-Weinberg condition. The coefficients of the couplings of the charged scalars H^\pm are the same as those of the pseudo-scalar A .

2.1 Decays to the SM-like Higgs

In addition to the couplings involving one scalar, we will be interested in three couplings involving two or more scalars: the coupling of h to the pseudoscalar A and a Z boson, g_{hZA} ; the coupling of h to the charged Higgs H^\pm and a W boson, $g_{hW^\mp H^\pm}$; and the coupling of the heavy Higgs scalar H to two SM-like scalars h : g_{Hhh} . These control the rates of the three processes $A \rightarrow Zh, H^\pm \rightarrow W^\pm h$, and $H \rightarrow hh$ that may be kinematically available when $m_h < m_A \sim m_H \sim m_{H^\pm}$.

The couplings of two scalars to a SM vector are transparently written in terms of departure from the alignment limit. In particular, we have

$$g_{hZA} = \frac{1}{2} \sqrt{g^2 + g'^2} \cos(\beta - \alpha) \quad g_{hW^\mp H^\pm} = \mp \frac{i}{2} g \cos(\beta - \alpha) \quad (2.8)$$

The form of these couplings is guaranteed by unitarity constraints. In a 2HDM the couplings g_{hZA}, g_{HZA} and $g_{hW^\mp H^\pm}, g_{HW^\mp H^\pm}$ obey a unitarity constraint akin to that satisfied by g_{hVV}, g_{HVV} , namely

$$g_{hZA}^2 + g_{HZA}^2 = \frac{1}{4m_Z^2} g_{h_{\text{SM}}ZZ}^2 \quad (2.9)$$

$$g_{hW^\mp H^\pm}^2 + g_{HW^\mp H^\pm}^2 = g_{AW^\mp H^\pm}^2 = \frac{1}{4m_W^2} g_{h_{\text{SM}}WW}^2 \quad (2.10)$$

Unlike the other couplings involving SM vectors or fermions, the triple Higgs coupling g_{Hhh} depends on additional parameters beyond the physical masses and mixing angles. As

we show in detail in Appendix A, this coupling is conveniently expressed as a function of the physical masses, the mixing angles, and the quartic couplings $\lambda_5, \lambda_6, \lambda_7$; in terms of $\tan \beta$ and $\beta - \alpha$ it is given by

$$\begin{aligned}
g_{Hhh} = \frac{\cos(\beta - \alpha)}{v} & \left[(3m_A^2 + 3\lambda_5 v^2 - 2m_h^2 - m_H^2) \left(\cos(2\beta - 2\alpha) - \frac{\sin(2\beta - 2\alpha)}{\tan(2\beta)} \right) \right. \\
& - m_A^2 - \lambda_5 v^2 + \frac{\lambda_6 v^2}{2} (-\cot \beta + 3 \sin(2\beta - 2\alpha) + 3 \cot \beta \cos(2\beta - 2\alpha)) \\
& \left. + \frac{\lambda_7 v^2}{2} (-\tan \beta - 3 \sin(2\beta - 2\alpha) + 3 \tan \beta \cos(2\beta - 2\alpha)) \right] \quad (2.11)
\end{aligned}$$

Various simplifying limits are presented in Appendix A.

There are a number of key points worth emphasizing about the coupling g_{Hhh} and the corresponding partial width for $H \rightarrow hh$. Note that $g_{Hhh} \propto \cos(\beta - \alpha)$ so that in the exact alignment limit $g_{Hhh} \rightarrow 0$. Indeed, g_{Hhh} approaches zero in the alignment limit at the same rate as the vector coupling g_{HVV} , so that neither $H \rightarrow hh$ nor $H \rightarrow VV$ is available when h is exactly SM-like. However, these processes may be important even if deviations from the alignment limit are small, and in fact may dominate the total width of H since both partial widths grow as $\Gamma(H \rightarrow VV, hh) \propto m_H^3/v^2$. Which of the two processes dominates is then a matter of numerical coefficients. Significantly, it is often the case that $\Gamma(H \rightarrow hh) \gtrsim \Gamma(H \rightarrow VV)$ when kinematically open, in which case $H \rightarrow hh$ dominates over $H \rightarrow VV$. Note that g_{Hhh} grows at large and small $\tan \beta$, but only well away from the alignment limit, as in the limit of small $\cos(\beta - \alpha)$ the leading $\tan \beta$ - and $\cot \beta$ -enhanced terms in g_{Hhh} scale as $\cos^2(\beta - \alpha)$. Away from the exact alignment limit, at large $\tan \beta$ we have $\Gamma(H \rightarrow hh) \gg \Gamma(H \rightarrow VV)$ due to the $\tan \beta$ enhancement of $\Gamma(H \rightarrow hh)$. This is important in determining the optimal search channels for the heavier Higgs H as m_H is varied, since it implies that $\text{Br}(H \rightarrow VV)$ may be small even when the partial width is appreciable. Of course, there are some exceptions; g_{Hhh} approaches zero as $\sin(\beta - \alpha) \rightarrow 1$ and also when $\cos(2\beta - 2\alpha) - \frac{\sin(2\beta - 2\alpha)}{\tan(2\beta)} \approx \frac{1}{2} \frac{1}{1 - m_h^2/m_H^2}$, where the decay $H \rightarrow VV$ may dominate instead.

It is an oft-repeated truism that $H \rightarrow hh$ is unimportant at large $\tan \beta$ in a Type 2 2HDM because the $\tan \beta$ -enhanced coupling of H to bottom quarks rapidly leads to $\Gamma(H \rightarrow b\bar{b})$ taking over the total width. This is true to a certain extent when $\lambda_6 = \lambda_7 = 0$, in which case the leading contributions to g_{Hhh} near the alignment limit are not enhanced by $\tan \beta$ and $\tan \beta$ -enhanced terms first arise at $\mathcal{O}(\cos^2(\beta - \alpha))$. The bottom coupling y_{Hbb} is $\tan \beta$ -enhanced, however, and so rapidly takes over the total width as $\tan \beta$ is increased, suppressing the $H \rightarrow hh$ branching ratio. (Note that this is not an issue in Type 1 2HDM, where there are no $\tan \beta$ -enhanced couplings and $H \rightarrow hh$ continues to dominate the total width at large $\tan \beta$.) However, even in Type 2 2HDM this ceases to be the case when λ_6 and λ_7 are nonzero. Near the alignment limit, the leading $\tan \beta$ -enhanced contribution to g_{Hhh} scales as $\sim 2\lambda_7 v \tan \beta \cos(\beta - \alpha)$. This may easily compete with the $\tan \beta$ enhancement of y_{Hbb} , in which case $H \rightarrow hh$ continues to govern the total width even when $\tan \beta$ is large. While we will not study the consequences of nonzero $\lambda_{6,7}$ extensively in what follows, it bears emphasizing

that when $\lambda_{6,7}$ are non-vanishing $H \rightarrow hh$ may dominate the total width even in cases where fermion couplings are parametrically enhanced.

Given this simplified parameter space for theories with two Higgs doublets, we can fit the current signals of the SM-like Higgs h in terms of α and β and then map this fit onto the range of production and decay rates for additional scalars.

3 Couplings of the SM-like Higgs

In order to ascertain which production and decay modes may be promising in future LHC searches, we first construct fits to the signals of the SM-like Higgs in terms of the 2HDM parameter space.⁶ The fit to SM-like Higgs couplings is constructed with all of the most recent available data from the LHC and Tevatron. We use fully exclusive channel breakdowns, as required for correct identification of the couplings controlling a given mode’s production cross-section. The profile of the signal strength modifier for each channel is fit with a two-sided Gaussian when best fit information is provided, otherwise we rely on likelihood reconstruction techniques reviewed in [52].

In Fig. 1 we show the total global fits for all four discrete 2HDM types as a function of α and β . From these fits it is strongly apparent that all four types favor the alignment limit $\beta - \alpha = \pi/2$. The fits in Type 2 and Type 4 2HDM models are particularly tight around the alignment limit due to the variation in the bottom quark coupling, as we will discuss in detail below. It is apparent that Types 2-4 all feature a second lobe of the fit away from the alignment limit with $\alpha > 0$, corresponding to changing the sign of g_{hVV} relative to the fermion couplings. This region was favored by previous fits to 2HDM couplings due to enhanced values of $h \rightarrow \gamma\gamma$ observed by both ATLAS and CMS in early Higgs data. However, the most recent CMS measurement of $h \rightarrow \gamma\gamma$ falls below the SM rate, so that this region is no longer favored by the combined fit. Note that the region with $\alpha > 0$ is not allowed in the specific Type 2 2HDM corresponding to the MSSM Higgs sector.

In light of the evident preference for the alignment limit, in Figs. 2 and 3 we show respectively the total global fits for 2HDMs of Type 1 and 2 around the alignment limit as a function of β and $\cos(\beta - \alpha)$. In addition to showing the combined fit, we also indicate how the different final states $\gamma\gamma, WW, ZZ, \tau\tau$, and bb contribute individually to the combined fit in order to illustrate the interplay between different 2HDM couplings governing the shape of the fits. For reference, in Table 3 we quote values of the quantity $\cos(\beta - \alpha)$ at the 95% CL contour for three benchmark values of $\tan\beta$.

We can gain some intuition for the shape of the coupling fits as a function of α and β by considering how couplings and rates scale in the limits of small and large values of β in each case.

For Type 1 2HDM, we have the following important limits to consider:

⁶For a partial list of recent work on Higgs coupling fits at the LHC, see e.g. [34, 37–51].

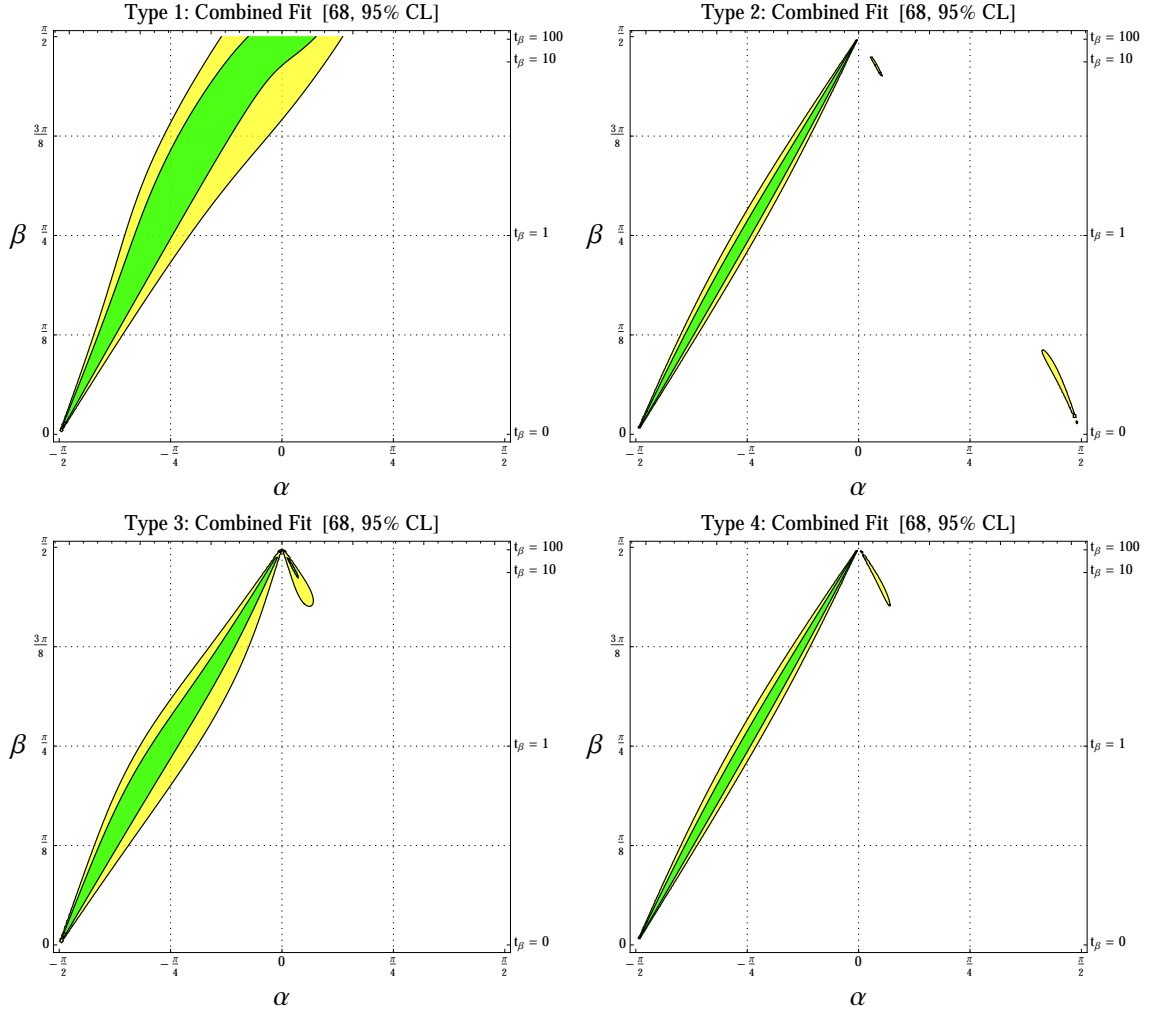


Figure 1. Upper left: Global fit of SM-like Higgs couplings in 2HDM of Type 1. Upper right: Global fit of SM-like Higgs couplings in 2HDM of Type 2. Lower left: Global fit of SM-like Higgs couplings in 2HDM of Type 3. Lower right: Global fit of SM-like Higgs couplings in 2HDM of Type 4.

- At large $\tan \beta$, the couplings scale very simply, namely

$$c_V, c_t, c_b, c_\tau \rightarrow \cos \alpha \quad (3.1)$$

where $c_V \equiv y_{hVV}/y_{h_{SM}VV}$, $c_t \equiv y_{hQu}/y_{h_{SM}Qu}$, $c_b \equiv y_{hQd}/y_{h_{SM}Qd}$, and $c_\tau \equiv y_{hLe}/y_{h_{SM}Le}$. Thus all rates are rescaled equally, such that along the $\tan \beta = \infty$ line the fit region corresponds to a best fit on a simple one-dimensional signal strength modifier.

- At small $\tan \beta$, the couplings scale instead as

$$c_V \rightarrow -\sin \alpha \quad (3.2)$$

$$c_t, c_b, c_\tau \rightarrow \beta^{-1} \cos \alpha. \quad (3.3)$$

Model	$\tan \beta$	$(c_{\beta-\alpha})_-^{95\%}$	$(c_{\beta-\alpha})_+^{95\%}$
Type 1	1	-0.32	0.42
	10	-0.43	0.40
	100	-0.42	0.13
Type 2	1	-0.11	0.06
	10	-0.02	0.01
	100	—	—

Table 3. Values of $\cos(\beta - \alpha)$ on positive and negative sides of the alignment limit, denoted by subscripts \pm , at the 95% CL contour for various values of $\tan \beta$. For Type 2 2HDM, at very large values of $\tan \beta$ the width of the region in $\cos(\beta - \alpha)$ allowed by measured coupling values of the SM-like Higgs is narrower than the resolution of our fit procedure; see Fig. 3.

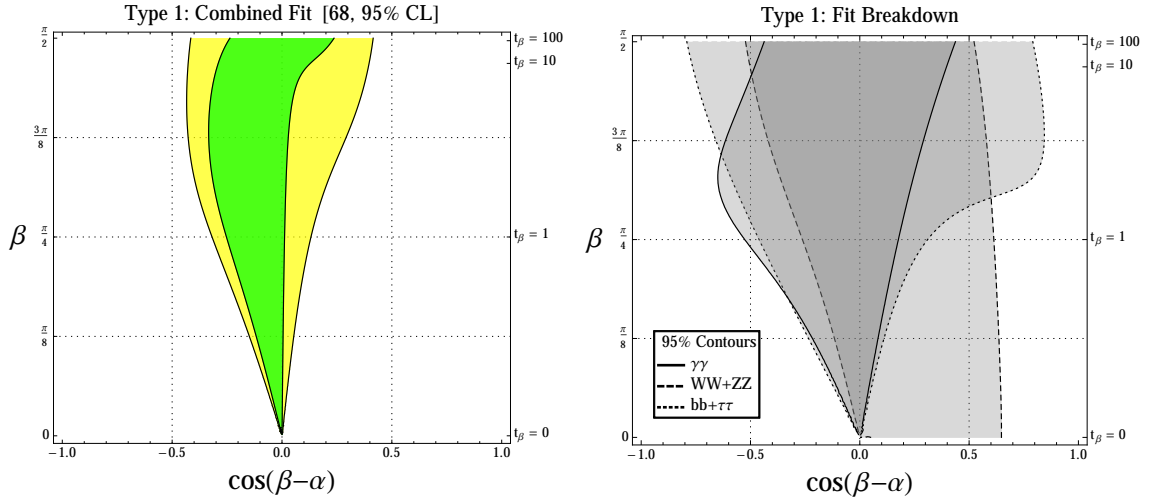


Figure 2. Left: Global fit of SM-like Higgs couplings in 2HDM of Type 1. Right: Contributions to the fit coming separately from $h \rightarrow \gamma\gamma$, $h \rightarrow VV$, and $h \rightarrow bb, \tau\tau$.

Assuming the fermion couplings dominate the total width, the rates of the important

individual channels therefore get rescaled in simple ways:

$$R_{\gamma\gamma} \approx \frac{\sigma(gg \rightarrow h) \times \text{BR}(h \rightarrow \gamma\gamma)}{\sigma(gg \rightarrow h_{SM}) \times \text{BR}(h_{SM} \rightarrow \gamma\gamma)} \sim c_t^2 \times \frac{c_V^2}{c_b^2} \rightarrow \sin^2 \alpha \quad (3.4)$$

$$R_{VV} \approx \frac{\sigma(gg \rightarrow h) \times \text{BR}(h \rightarrow VV^*)}{\sigma(gg \rightarrow h_{SM}) \times \text{BR}(h_{SM} \rightarrow VV^*)} \sim c_t^2 \times \frac{c_V^2}{c_b^2} \rightarrow \sin^2 \alpha \quad (3.5)$$

$$R_{bb}^{(Vh)} = \frac{\sigma(pp \rightarrow Vh) \times \text{BR}(h \rightarrow bb)}{\sigma(pp \rightarrow Vh_{SM}) \times \text{BR}(h_{SM} \rightarrow bb)} \sim c_V^2 \times \frac{c_b^2}{c_b^2} \rightarrow \sin^2 \alpha \quad (3.6)$$

$$R_{bb}^{(t\bar{t}H)} = \frac{\sigma(pp \rightarrow t\bar{t}h) \times \text{BR}(h \rightarrow bb)}{\sigma(pp \rightarrow t\bar{t}h_{SM}) \times \text{BR}(h_{SM} \rightarrow bb)} \sim c_t^2 \times \frac{c_b^2}{c_b^2} \rightarrow \beta^{-2} \cos^2 \alpha \quad (3.7)$$

$$R_{\tau\tau}^{(VBF)} = \frac{\sigma(pp \rightarrow hjj) \times \text{BR}(h \rightarrow \tau\tau)}{\sigma(pp \rightarrow h_{SM}jj) \times \text{BR}(h_{SM} \rightarrow \tau\tau)} \sim c_V^2 \times \frac{c_\tau^2}{c_b^2} \rightarrow \sin^2 \alpha \quad (3.8)$$

$$R_{\tau\tau}^{(\text{inc.})} \approx \frac{\sigma(gg \rightarrow h) \times \text{BR}(h \rightarrow bb)}{\sigma(gg \rightarrow h_{SM}) \times \text{BR}(h_{SM} \rightarrow bb)} \sim c_t^2 \times \frac{c_\tau^2}{c_b^2} \rightarrow \beta^{-2} \cos^2 \alpha \quad (3.9)$$

Thus we can easily understand why the diphoton contour narrows at small β while the VV mode, whose VBF-initiated contribution vanishes in this limit, occupies a finite region of the $\beta = 0$ line. The asymmetry in the VV contour at small β reflects the fact that $\cos \alpha > 0$ by definition.

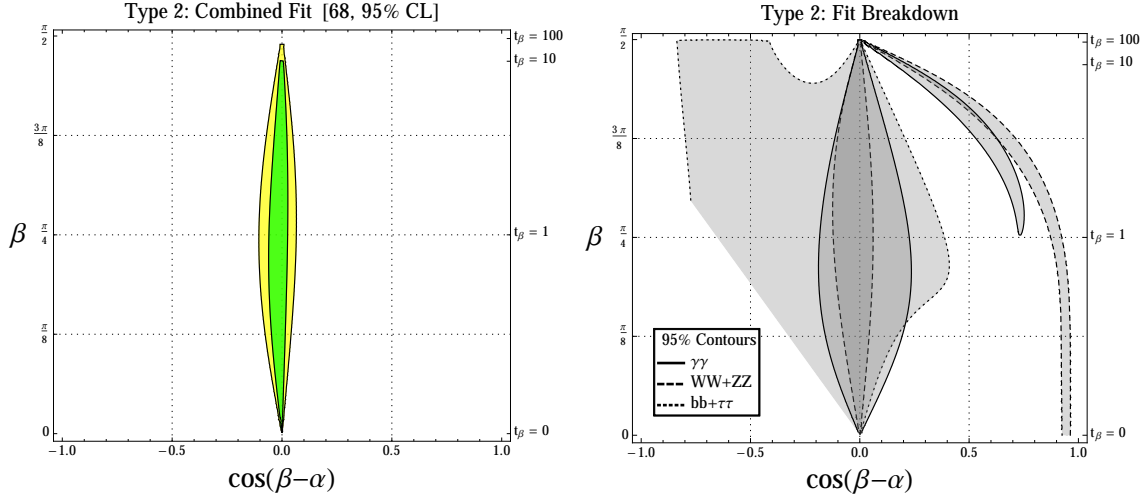


Figure 3. Left: Global fit of SM-like Higgs couplings in 2HDM of Type 2. Right: Contributions to the fit coming separately from $h \rightarrow \gamma\gamma$, $h \rightarrow VV$, and $h \rightarrow bb, \tau\tau$. The peninsulas of the $\gamma\gamma$ and VV contours correspond to regions where the bottom coupling has changed sign (i.e. $\alpha > 0$) and has a magnitude that is respectively suppressed/unsuppressed relative to the decoupling limit (see Type 2 SM-like Higgs decay rates in Figs. 4, 5, 6 for comparison). Note also that the apparent discontinuity in the $bb + \tau\tau$ contour arises from the requirement $\alpha > -\pi/2$.

In the Type 2 2HDM case we see a more dynamic interplay between the separate channels, with VV providing a powerful constraint due to its sensitivity to the vector coupling. We note the following limiting behaviors:

- At large β , we have

$$c_V, c_t \rightarrow \cos \alpha \quad (3.10)$$

$$c_b, c_\tau \rightarrow \frac{1}{\beta - \pi/2} \times \sin \alpha \quad (3.11)$$

Rates for each channel thus scale as follows:

$$R_{\gamma\gamma}, R_{VV} \rightarrow \left(\beta - \frac{\pi}{2}\right)^2 \frac{\cos^4 \alpha}{\sin^2 \alpha} \quad (3.12)$$

$$R_{bb}, R_{\tau\tau} \rightarrow \cos^2 \alpha \quad (3.13)$$

Thus the $\gamma\gamma$ and VV likelihoods vanish, while bb and $\tau\tau$ remain finite at large β . Notice that cancellation between large couplings (c_b, c_τ) in branching fractions is accurate only asymptotically, or in regions of parameter space where the vector coupling and top coupling are significantly diminished. Incidentally, this is the reason for the slight depression in the $bb/\tau\tau$ fit contour at large β and small $\cos(\beta - \alpha)$, where values of vector and top couplings remain near their SM values.

- At small β the couplings scale as

$$c_V, c_b, c_\tau \rightarrow -\sin \alpha \quad (3.14)$$

$$c_t \rightarrow \beta^{-1} \cos \alpha \quad (3.15)$$

Likelihoods therefore tend to vanish at small β since rates become arbitrarily large, i.e.

$$R_{\gamma\gamma}, R_{VV}, R_{bb}^{(ttH)}, R_{\tau\tau}^{(inc.)} \rightarrow \beta^{-2} \cos^2 \alpha \quad (3.16)$$

$$R_{bb}^{(VH)}, R_{\tau\tau}^{(VBF)} \rightarrow \sin^2 \alpha \quad (3.17)$$

Notice also that the diphoton contour shows some mild preference for positive values of $\cos(\beta - \alpha)$. In this region of the fit the bottom coupling is suppressed relative to the SM, thus allowing an enhanced $\gamma\gamma$ from the reduced $b\bar{b}$ branching fraction; this is the region that would be favored by current diphoton results from ATLAS [53]. This contour is cut off at small β by an excessive top coupling (and thus excessive production via gluon fusion); at somewhat larger β it is cut off by the reduction in the bottom coupling's magnitude overshooting the preferred enhancement in diphoton. Additional channels sensitive to the vector coupling therefore become important in shaping the combined fit contour for these intermediate values of β .

With these coupling fits in hand, we may investigate the prospects for evidence of extended electroweak symmetry breaking by studying the range of variations in SM-like Higgs couplings that remain poorly constrained by present measurements as well as the range of signals available to the heavier scalars H , A , and H^\pm .

4 Signals of the Second Higgs Doublet

At present, the coupling fits of the SM-like Higgs are dominated by a few signal channels that have meaningful sensitivity in the discovery-level data set. Beyond these channels, there are a variety of signal channels whose measurements are poorly constrained at present but will improve with additional integrated luminosity. This makes it useful to study the possible variation in future measurements consistent with current fits. Deviations in these channels may provide the first indication of the presence of additional Higgs scalars. Of course, these additional scalars may also be observed directly, either in standard Higgs search channels or through cascade decays involving multiple scalars. Coupling fits of the SM-like Higgs serve to pick out the most promising of these discovery channels.

In what follows, we will explore the range of 2HDM signals in various modes consistent with current best fits to the SM-like Higgs couplings. To do so, we adopt the following procedure to determine the appropriate product of production cross section times branching ratio:

For the case of the SM Higgs boson, we take the NLO production cross sections for gluon fusion, vector boson fusion, and production in association with a vector boson or top quarks from the LHC Higgs Cross Section Working Group [54]. For 2HDM, we calculate the ratio of LO production partial widths in each production channel for h and H relative to a SM Higgs boson of the same mass analytically from the couplings presented in Section 2 as functions of the mixing parameters α and β . The NLO SM Higgs production cross sections in each production channel are then rescaled by these factors to obtain an estimate for the NLO cross sections; for instance we take the α, β dependent cross section for gluon fusion production of H to be

$$\sigma_{\text{NLO}}(gg \rightarrow H)|_{\alpha, \beta} = \sigma_{\text{NLO}}(gg \rightarrow h_{\text{SM}}) \frac{\Gamma_{\text{LO}}(H \rightarrow gg)|_{\alpha, \beta}}{\Gamma_{\text{LO}}(h_{\text{SM}} \rightarrow gg)} \quad (4.1)$$

where H and h_{SM} are of the same mass. The same procedure of normalizing to SM Higgs boson NLO cross sections through the α and β dependent ratios of LO production partial widths is used for production of A by gluon fusion or in association with top quarks. This is expected to be a good approximation since the fractional size of NLO corrections in these cases is not strongly dependent on the parity of the Higgs scalar away from the two-top threshold. Near the two-top threshold the NLO corrections to the pseudoscalar production cross section are larger than the NLO corrections to the scalar cross section, so our procedure is conservative.

Although the cross section for production of a SM Higgs boson in association with bottom quarks is quite small, it may play an important role in 2HDM with enhanced bottom couplings. In order to account for these contributions, we obtain the inclusive NLO production cross section $\sigma(pp \rightarrow (b\bar{b})h_{\text{SM}} + X)$ for a SM Higgs boson produced via $b\bar{b}$ annihilation using `bbh@nlo` [55] with the choice of equal factorization and renormalization scales: $\mu_F = \mu_R = m_h/4$. Note that `bbh@nlo` computes the inclusive cross section $\sigma(pp \rightarrow (b\bar{b})h_{\text{SM}} + X)$ in a variable flavor number scheme in which the LO partonic process is $b\bar{b} \rightarrow h_{\text{SM}}$; the corresponding cross

section does not include any tagging requirements on bottom quarks in the final state. To obtain the 2HDM NLO cross sections for this process we rescale the NLO SM Higgs production cross section by the ratio of LO partial widths as above.

We will often be interested in the “inclusive” production cross section for a given Higgs state. In practice, the experimental measurement of an inclusive Higgs process assigns different weights to various production modes. In the case of current measurements at the LHC, these weights are known and are used appropriately in determining the coupling fits in Section 3. However, the weights for many future measurements are unknown, and so in this section we approximate inclusive production rates by summing the appropriate production cross sections without any relative re-weighting due to differences in experimental acceptance.

Our procedure for decay modes is analogous. For the case of the SM Higgs boson, the NLO partial decay widths and branching ratios are taken from the LHC Higgs Cross Section Working Group [54]. For the 2HDM spectra the ratio of LO partial decay widths for h relative to a SM Higgs boson of the same mass are calculated analytically as functions of the mixing parameters α and β using the couplings presented above. The NLO SM Higgs boson partial decay widths are then rescaled by these factors to obtain estimates for the NLO partial widths; for instance we take the α, β dependent partial width for the SM-like Higgs h to $b\bar{b}$ to be

$$\Gamma_{\text{NLO}}(h \rightarrow b\bar{b})|_{\alpha,\beta} = \Gamma_{\text{NLO}}(h_{\text{SM}} \rightarrow b\bar{b}) \frac{\Gamma_{\text{LO}}(h \rightarrow b\bar{b})|_{\alpha,\beta}}{\Gamma_{\text{LO}}(h_{\text{SM}} \rightarrow b\bar{b})} \quad (4.2)$$

The same procedure of normalizing to SM Higgs boson NLO partial decay widths through the ratio of LO decay widths is used for the H decay modes that are in common with the h decay modes. For the pseudoscalar A , we instead use analytic results for the NLO partial widths into fermions as a function of α and β [56] since the parity of the pseudoscalar is particularly important near the fermion pair thresholds. For the charged Higgs H^\pm we simply use the analytic results for the LO partial widths into fermions as a function of α and β [57]. For the decay modes $H \rightarrow hh$ and $A \rightarrow Zh$ we use the analytic results for LO partial widths [58] as a function of α and β . None of these decay modes involves strongly interacting particles, so LO widths are a reasonable approximation. The partial widths for all the open decay modes of each Higgs scalar are then used to calculate the α and β dependent total widths and branching ratios.

Note that certain processes such as $H \rightarrow hh$ and $A \rightarrow Zh$ constitute additional sources of production for the SM-like Higgs. In this work we do not simultaneously incorporate these potential new sources of h production into the coupling fit. This is a reasonable approximation insofar as the acceptance for these production modes is currently unknown and, in general, the $\lesssim \mathcal{O}(\text{pb})$ cross-sections involved should not significantly distort the coupling fit given the signal channels that currently dominate the couplings. However, as sensitivity to Vh exclusive production improves with additional integrated luminosity, a simultaneous fit to SM-like and heavy scalar production would be useful.

Throughout, we will neglect loop-level contributions from H^\pm to the $h, H \rightarrow \gamma\gamma$ rates. These contributions are suppressed relative to W and top loops by a factor of $\mathcal{O}(m_W^2/m_{H^\pm}^2)$ and decouple particularly rapidly near the alignment limit [36].

5 Signs of the Second Higgs Doublet in the SM-like Higgs Couplings

Current signals are dominated by inclusive and VBF production of h with $h \rightarrow \gamma\gamma$ as well as inclusive production of h with $h \rightarrow VV^*$. Sensitivity in inclusive and Vh /VBF associated production of h with $h \rightarrow \tau^+\tau^-$ and Vh production of h with $h \rightarrow b\bar{b}$ is improving, but the errors on these measurements remain large. There are also a variety of inclusive and associated measurements that may be made using the future LHC data set, but for which there is currently no sensitivity. Thus it is instrumental to consider the range of signals that might be anticipated in the following future measurements given the state of current fits:

- Inclusive production of h with $h \rightarrow \tau^+\tau^-$ or $h \rightarrow \mu^+\mu^-$
- Vh /VBF production of h with $h \rightarrow \tau^+\tau^-$
- Vh production of h with $h \rightarrow b\bar{b}$
- Vh /VBF production of h with $h \rightarrow \gamma\gamma$
- Vh /VBF production of h with $h \rightarrow VV^*$
- Inclusive production of h with $h \rightarrow Z\gamma$
- $t\bar{t}$ associated production of h with $h \rightarrow \gamma\gamma$

The parametric dependence of the production cross section times branching ratio on α and β for each of these processes may be understood by considering the functional dependence of the production mode, the decay mode, and the total width. While the scaling of decay modes is fairly straightforward, the production mode and total width are slightly more subtle. In Type 1 and 3 2HDM, the production modes are fairly simple; Vh and VBF associated production scale as c_V^2 , while inclusive production is dominated by gluon fusion and scales as c_t^2 . In Type 2 and 4 2HDM, however, at large $\tan\beta$ the inclusive production is dominated by $b\bar{b}h$ associated production, and the parametrics switch over from $\propto c_t^2$ to $\propto c_b^2$. As for branching ratios, the decay mode is unambiguous but the dominant contribution to the total width may vary. In general, the dominant contributions to the total width come from the partial widths $\Gamma(h \rightarrow b\bar{b})$ and $\Gamma(h \rightarrow VV^*)$. Unsurprisingly, $\Gamma(h \rightarrow b\bar{b})$ dominates over much of the parameter space, but becomes sub-dominant in specific regions where $c_b \rightarrow 0$, which vary depending on the 2HDM type. For Type 1 and Type 3 2HDM, $c_b \rightarrow 0$ as $\alpha \rightarrow \pm\frac{\pi}{2}$. For Type 2 and Type 4 2HDM, $c_b \rightarrow 0$ as $\alpha \rightarrow 0$. In these regions, the contribution of $\Gamma(h \rightarrow b\bar{b})$ to the total width vanishes, and the parametric dependence of the total width is instead dominated by $\Gamma(h \rightarrow VV^*)$. Thus the parametric scaling of the total width is

generally dominated by the scaling of c_b^2 , except in special regions where $c_b \rightarrow 0$ and the width is instead dominated by c_V^2 . In general these regions are disfavored by current fits.

The parametrics of many of these channels as a function of α and β in the four types of 2HDM were discussed in detail in [3] and above in Section 3; here we focus on the specific channels in which future deviations may arise.

5.1 Inclusive production of h with $h \rightarrow \tau^+\tau^-$ or $h \rightarrow \mu^+\mu^-$

The measurement of the inclusive $h \rightarrow \tau^+\tau^-$ rate is improving in sensitivity at both ATLAS and CMS, but there remains substantial room for deviations. The inclusive $h \rightarrow \mu^+\mu^-$ rate has identical parametric scaling in the 2HDM we consider, and at present is very poorly constrained at the LHC.

Contours of the inclusive ratio $\sigma \cdot \text{Br}(h \rightarrow \tau^+\tau^-)/\sigma \cdot \text{Br}(h_{SM} \rightarrow \tau^+\tau^-)$ are shown in Fig. 4. The inclusive rates scale identically for both lepton flavors over the bulk of the 2HDM parameter space, $\sim c_t^2 \times c_\tau^2/c_b^2$ except where $c_b \rightarrow 0$ and $\Gamma(h \rightarrow VV^*)$ takes over the total width. Thus in Type 1 models, around the alignment limit the inclusive rate scales as $\sim 1 + 2\frac{\cos(\beta-\alpha)}{\tan\beta}$ and may be raised or lowered relative to the SM rate depending on the sign of $\cos(\beta - \alpha)$. The region of suppressed rate for $\cos(\beta - \alpha) < 0$ corresponds to $\alpha = -\pi/2$ where $c_b, c_\tau \rightarrow 0$ and is disfavored by current fits.

In Type 2 models, for moderate $\tan\beta$ the inclusive rate scales similarly around the alignment limit, since any increase in coupling to leptons is offset by an increase in the total width due to enhanced bottom couplings. At large $\tan\beta$, however, enhanced bottom couplings begin to dominate production modes (primarily through $b\bar{b}h$ production) and the scaling at large $\tan\beta$ scales as $\sim 1 - 2\cos(\beta - \alpha)\tan\beta$. The region of suppressed rate for $\cos(\beta - \alpha) > 0$ corresponds to $\alpha = 0$ where $c_b, c_\tau \rightarrow 0$ and unsurprisingly is disfavored by current fits.

In Type 3 models, the parametric scaling of production rates and total width cancel, leaving the enhancement of the lepton couplings to dominate the signal $\sim 1 - 2\cos(\beta - \alpha)\tan\beta$. In Type 4 models, the scaling is $\sim 1 + 4\frac{\cos(\beta-\alpha)}{\tan\beta} + 2\cos(\beta - \alpha)\tan\beta$.

In general, there is not much room for significant deviations in the inclusive $h \rightarrow \tau^+\tau^-$ and $h \rightarrow \mu^+\mu^-$ rates given relatively good limits on the fermionic couplings of the Higgs. In Type 1 (3) models there may be $\mathcal{O}(50\%)$ suppression (enhancement) of the inclusive rate consistent with the 68 % CL best fit, but in Type 2 and Type 4 models the remaining room for deviations is not more than $\mathcal{O}(20\%)$ above or below the SM rate, which is smaller than the current sensitivity in this channel.

5.2 Vh /VBF production of h with $h \rightarrow \tau^+\tau^-$

Measurement of $h \rightarrow \tau^+\tau^-$ in vector boson fusion currently has comparable sensitivity to the inclusive measurement, while $h \rightarrow \tau^+\tau^-$ in Vh associated production remains fairly poorly constrained due to the low rate. Contours of the exclusive ratio $\sigma \cdot \text{Br}(V\text{BF or }Vh \rightarrow \tau^+\tau^-)/\sigma \cdot \text{Br}(V\text{BF or }Vh_{SM} \rightarrow \tau^+\tau^-)$ are shown in Fig. 5. Both processes have the same parametric scaling in 2HDM, and the exclusive rates scale as $\sim c_V^2 \times c_\tau^2/c_b^2$ over most of the parameter space, with the above-mentioned features associated with $c_b, c_\tau \rightarrow 0$ lying outside

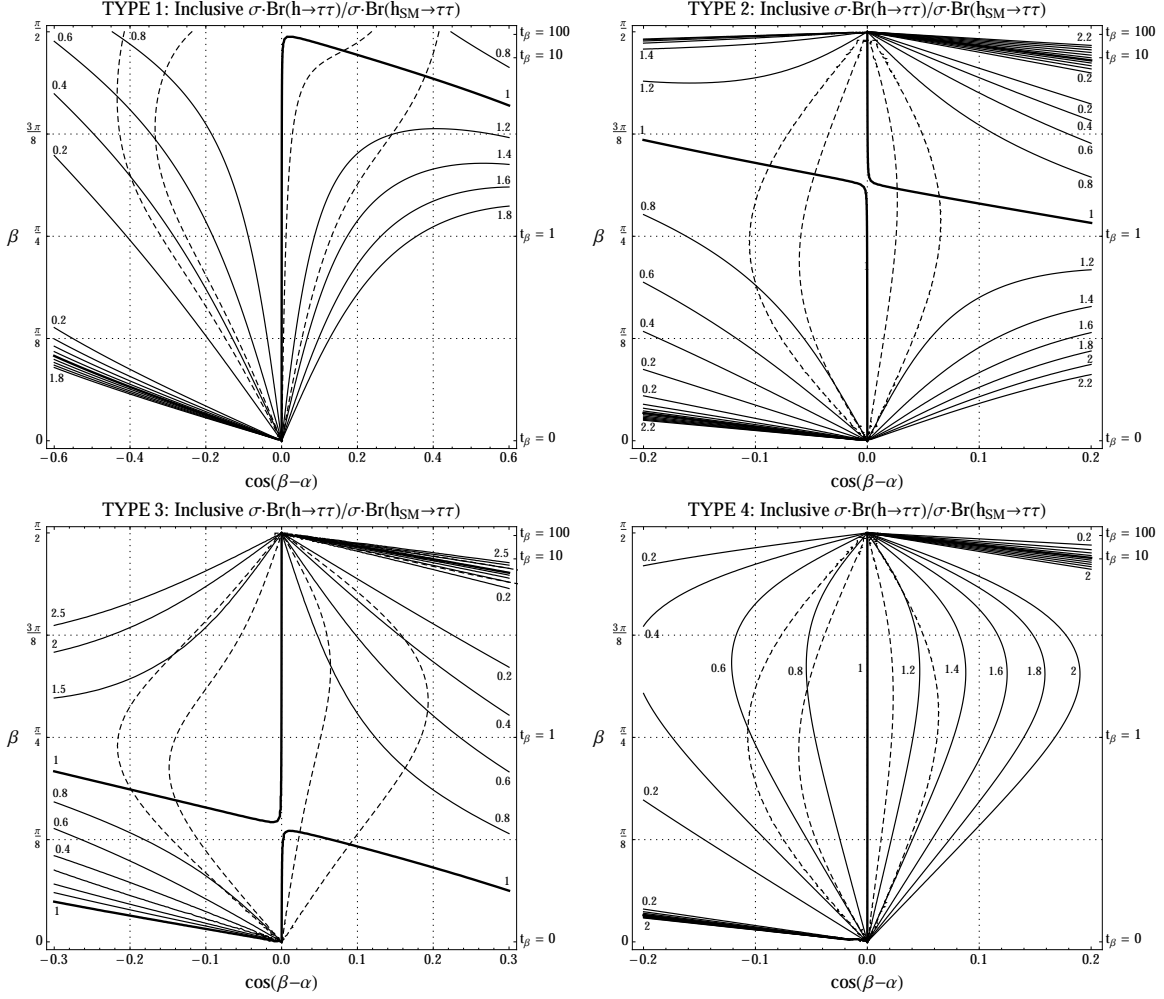


Figure 4. Contours of the inclusive $\sigma \cdot \text{Br}(h \rightarrow \tau^+\tau^-)/\sigma \cdot \text{Br}(h_{SM} \rightarrow \tau^+\tau^-)$ for 8 TeV pp collisions for the SM-like Higgs boson, shown as a function of $\cos(\beta - \alpha)$ and β for Type 1 (upper left), Type 2 (upper right), Type 3 (lower left), and Type 4 (lower right) 2HDM. The inner (outer) dashed contour denotes the 68% (95%) CL best fit to the signals of the SM-like Higgs.

the current best fit. In both Type 1 and Type 2 models this implies that the rates are constant at $\mathcal{O}(\cos(\beta - \alpha))$, and only vary significantly far from the alignment limit. Indeed, in both types the variation consistent with current fits is no more than $\sim \pm 20\%$ of the SM value.

However, in Type 3 and Type 4 models the parametric freedom is greater due to the difference between lepton and bottom quark couplings. In Type 3 models the inclusive rate scales as $1 - 2 \frac{\cos(\beta - \alpha)}{\tan \beta}$ at small $\tan \beta$ and as $1 - 2 \cos(\beta - \alpha) \tan \beta$ at large $\tan \beta$, allowing up to 50% enhancement of this exclusive rate consistent with the 68% fit. In Type 4 models the sign of the variation changes: $1 + 2 \frac{\cos(\beta - \alpha)}{\tan \beta}$ at small $\tan \beta$ and $1 + 2 \cos(\beta - \alpha) \tan \beta$ at large $\tan \beta$.

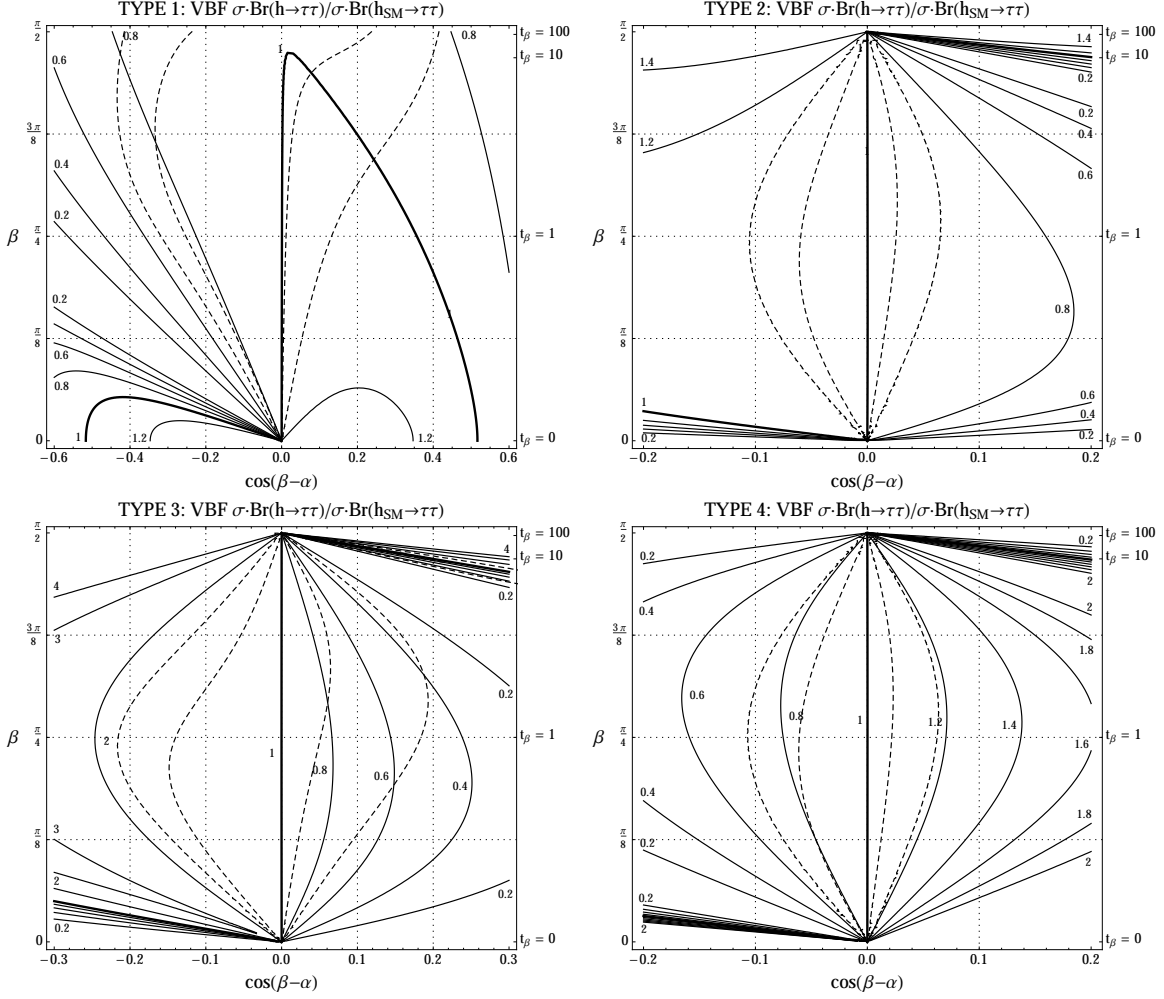


Figure 5. Contours of $\sigma \cdot \text{Br}(\text{VBF or } Vh \rightarrow \tau^+\tau^-) / \sigma \cdot \text{Br}(\text{VBF or } Vh_{\text{SM}} \rightarrow \tau^+\tau^-)$ for 8 TeV pp collisions for the SM-like Higgs boson, shown as a function of $\cos(\beta-\alpha)$ and β for Type 1 (upper left), Type 2 (upper right), Type 3 (lower left), and Type 4 (lower right) 2HDM. The inner (outer) dashed contour denotes the 68% (95%) CL best fit to the signals of the SM-like Higgs.

5.3 Vh production of h with $h \rightarrow b\bar{b}$

Measurement of Vh associated production of h with $h \rightarrow b\bar{b}$ remains challenging at the LHC and current direct limits are fairly loose. However, the exclusive rate for $b\bar{b}$ production scales identically to the rate for Vh production of h with $h \rightarrow \tau^+\tau^-$ in Type 1 and Type 2 models and are essentially constant near the alignment limit; contours are identical to those shown in Fig. 5. In fact, all four types of 2HDM scale similarly as long as $h \rightarrow b\bar{b}$ still dominates the total width of the Higgs.

5.4 Vh/VBF production of h with $h \rightarrow \gamma\gamma$

VBF production of h with $h \rightarrow \gamma\gamma$ is measured by both collaborations through dijet-tagged categories, but error bars remain fairly large. The 8 TeV data set allows preliminary measurements of Vh associated production with $h \rightarrow \gamma\gamma$, but current error bars are too large to place a meaningful constraint.

Contours of the exclusive ratio $\sigma \cdot \text{Br}(\text{VBF or } Vh \rightarrow \gamma\gamma)/\sigma \cdot \text{Br}(\text{VBF or } Vh_{SM} \rightarrow \gamma\gamma)$ are shown in Fig. 6. Both processes share the same parametric scaling in 2HDM. Unless the coupling to vectors is highly suppressed, the exclusive rates scale as $\sim c_V^2 \times c_V^2/c_b^2$ since the W loop dominates the effective $h\gamma\gamma$ coupling. In Type 1 models the parametric scaling is dominated by the change in the total width since $c_V \sim 1$, and so over the bulk of parameter space scales as $1 - 2 \frac{\cos(\beta-\alpha)}{\tan\beta}$. The region of enhancement for $\cos(\beta-\alpha) < 0$ again corresponds to $c_b, c_\tau \rightarrow 0$, but for this process it leads to an enhancement (rather than the suppression apparent in inclusive or VBF/ Vh production with $h \rightarrow \tau^+\tau^-$) because only the total width decreases while the production and decay modes remain constant. In Type 2 models the scaling is again dominated by the total width, $\sim 1 + 2 \cos(\beta-\alpha) \tan\beta$, and the region of enhancement for $\cos(\beta-\alpha) > 0$ corresponds to $c_b, c_\tau \rightarrow 0$ in analogy with the Type 1 case.

In Type 1 2HDM there is still considerable room for an enhanced rate of VBF production with $h \rightarrow \gamma\gamma$, with an enhancement by as much as $\sim 80\%$ consistent with the 68% CL fit. Although the recent CMS 8 TeV measurement of dijet-tagged diphoton categories now shows a deficit with respect to the SM, the CMS 7 TeV measurement and ATLAS 7 and 8 TeV measurements remain high, and this remains an interesting channel to probe in future measurements. In Type 2 2HDM the situation is much more tightly constrained, with no more than $\pm 20\%$ variation consistent with the 68% CL fit.

5.5 Vh/VBF production of h with $h \rightarrow VV^*$

Vh and VBF associated production of h with $h \rightarrow VV^*$ is currently poorly constrained by ATLAS and CMS, though both collaborations currently measure tagged categories for WW^* final states, and CMS now includes a dijet-tagged category for ZZ^* . These exclusive rates scale as $c_V^2 \times c_V^2/c_b^2$, much as the Vh/VBF production of h with $h \rightarrow \gamma\gamma$, and unsurprisingly the parametrics are essentially identical; we do not show them explicitly.

As with Vh/VBF production of h with $h \rightarrow \gamma\gamma$, in Type 1 2HDM there is room for up to $\sim 80\%$ enhancement in these channels consistent with the 68% CL fit. Should the VBF diphoton rate remain high, ancillary measurements in VBF and Vh with $h \rightarrow VV^*$ could provide a useful validation.

5.6 $t\bar{t}$ associated production of h with $h \rightarrow \gamma\gamma$

There is currently no meaningful measurement of $t\bar{t}$ associated production of h , though both ATLAS and CMS quote preliminary measurements of $t\bar{t}h$ with $h \rightarrow b\bar{b}$ with low sensitivity. The $t\bar{t}$ associated production of h with $h \rightarrow \gamma\gamma$ should be measurable with considerable integrated luminosity at 14 TeV. Contours of the exclusive $\sigma \cdot \text{Br}(t\bar{t}h \rightarrow \gamma\gamma)/\sigma \cdot \text{Br}(t\bar{t}h_{SM} \rightarrow$

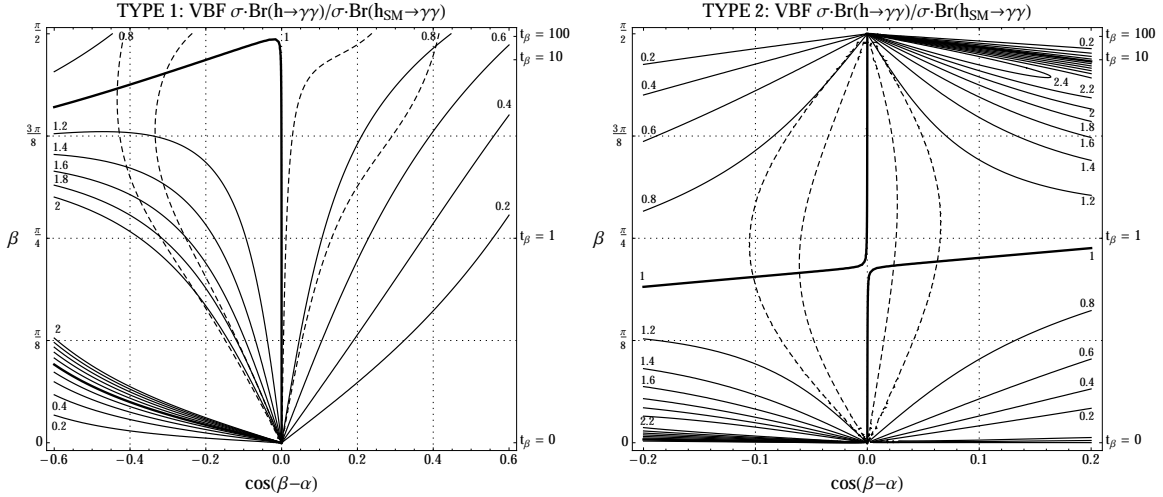


Figure 6. Contours of $\sigma \cdot \text{Br}(\text{VBF or } Vh \rightarrow \gamma\gamma) / \sigma \cdot \text{Br}(\text{VBF or } Vh_{SM} \rightarrow \gamma\gamma)$ for 8 TeV pp collisions for the SM-like Higgs boson, shown as a function of $\cos(\beta - \alpha)$ and β for Type 1 (left) and Type 2 (right) 2HDM. The inner (outer) dashed contour denotes the 68% (95%) CL best fit to the signals of the SM-like Higgs.

$\gamma\gamma$) ratio are shown in Fig. 7. The rate scales as $c_t^2 \times c_V^2 / c_b^2$ over much of the parameter space. These parametrics are similar to the parametrics for inclusive production with $h \rightarrow VV^*, \gamma\gamma$, and so unsurprisingly the signal contours trace the fit contours closely. In Type 1 2HDM this renders the rate flat around the alignment limit to $\mathcal{O}(\cos(\beta - \alpha))$, with mild modulation from sub-leading production modes. In Type 2 2HDM the parametric scaling around the alignment limit is $\sim 1 + 2 \frac{\cos(\beta - \alpha)}{\tan \beta} + 2 \cos(\beta - \alpha) \tan \beta$, so that the overall rate varies rapidly at large and small $\tan \beta$. This leaves little room for significant deviations in $t\bar{t}$ associated production of h with $h \rightarrow \gamma\gamma$ in these 2HDM.

5.7 Inclusive production of h with $h \rightarrow Z\gamma$

Inclusive production of h with $h \rightarrow Z\gamma$ is poorly constrained by current measurements, but may be measured at the 14 TeV LHC provided considerable integrated luminosity. The rate again scales as $c_t^2 \times c_V^2 / c_b^2$ over much of the parameter space since the $hZ\gamma$ coupling is dominated by vector loops, so that the contours of $h \rightarrow Z\gamma$ are similar to those of $t\bar{t}h$ with $h \rightarrow \gamma\gamma$ and trace the contours of the fit. Given the parametric similarity to $t\bar{t}h$ with $h \rightarrow \gamma\gamma$, we do not show the contours explicitly as a function of α and β . Since $h \rightarrow Z\gamma$ tracks the overall fit contours so closely, there is little room for substantial deviations from the SM prediction in these 2HDM.

5.8 Future prospects

For the most part, many decays of the SM-like Higgs that are poorly constrained by current data but measurable at 14 TeV are not expected to deviate significantly from the SM expectation, with typically $\pm 20\%$ deviation consistent with the current 68% CL coupling fits.

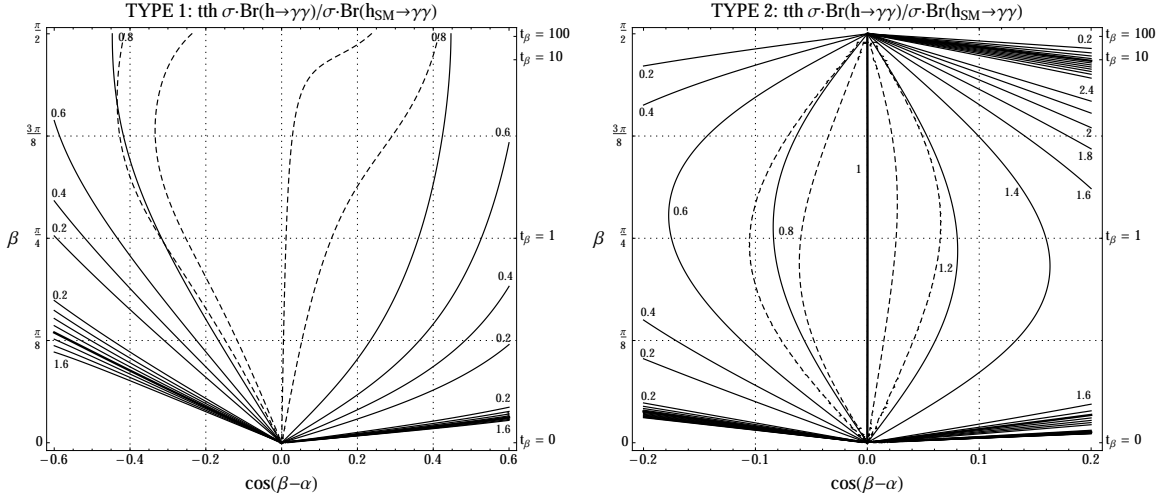


Figure 7. Contours of $\sigma \cdot \text{Br}(t\bar{t}h \rightarrow \gamma\gamma) / \sigma \cdot \text{Br}(t\bar{t}h_{SM} \rightarrow \gamma\gamma)$ for 8 TeV pp collisions for the SM-like Higgs boson, shown as a function of $\cos(\beta - \alpha)$ and β for Type 1 (left) and Type 2 (right) 2HDM. The inner (outer) dashed contour denotes the 68% (95%) CL best fit to the signals of the SM-like Higgs.

This is due to the fact that these modes scale similarly to well-measured production and decay modes that dominate the coupling fits. There are three notable exceptions in a Type 1 2HDM, which should be correlated in the event that substantial deviations are observed. An enhancement of up to $\sim 80\%$ in VBF or Vh associated production of h with $h \rightarrow \gamma\gamma, VV^*$ is consistent with the current 68% CL coupling fits at low $\tan\beta$. If such enhancement is present, it would be accompanied by as much as a 50% diminution in the inclusive $h \rightarrow \tau^+\tau^-$ rate, with the suppression in $h \rightarrow \tau^+\tau^-$ proportional to the enhancement in $h \rightarrow \gamma\gamma, VV^*$. The prospects are similar in a Type 3 2HDM, except that enhancement of VBF or Vh associated production with $h \rightarrow \gamma\gamma, VV^*$ would be accompanied by enhancement in both inclusive and exclusive processes with $h \rightarrow \tau^+\tau^-$.

Given that most remaining channels are fairly well constrained by current coupling fits, the possible direct signals of heavier Higgs scalars take on additional importance.

6 Direct Signs of the Second Higgs Doublet

In addition to looking for evidence of additional states through deviations from SM predictions for the couplings of the SM-like Higgs, it is instrumental to search directly for additional scalars, both in standard Higgs channels and in cascade decays involving multiple scalars. The most fruitful channels typically involve gluon fusion production of H and A , both because this offers a large production cross section and because the proximity to the alignment limit favored by current fits suppresses VBF and VH associated production of H . The production rate for H^\pm is small unless $m_{H^\pm} < m_t$, in which case H^\pm appears in $t\bar{t}$ pair production followed by the decay $t \rightarrow H^\pm b$. In this work we will not consider the case $m_{H^\pm} < m_t$, where there is a small rate for $t\bar{t}H^\pm$ associated production.

To illustrate the possible range of branching ratios as a function of mass consistent with current coupling fits, we first choose benchmark values of α and β corresponding to the 95% CL boundary of the Higgs fits as shown in Table 3 and plot the inclusive production cross section times branching ratios as a function of m_H or m_A . Although many cascade decays are possible among scalars, in the limit $m_h < m_A \sim m_H \sim m_{H^\pm}$ there is a natural ordering of available decay modes when kinematically available; only $H \rightarrow hh$, $A \rightarrow Zh$, and $H^\pm \rightarrow W^\pm h$ are open. In what follows we assume this approximate mass ordering and neglect other possible decays among scalars. Fig. 8 shows the cross section times branching ratios of H as a function of m_H in Type 1 and Type 2 2HDM for two reference points: a “low $\tan\beta$ ” point with $\tan\beta = 1$ and $\cos(\beta - \alpha)$ on the boundary of the 95% CL fit, and a “high $\tan\beta$ ” point with $\tan\beta = 10$ and $\cos(\beta - \alpha)$ again on the boundary of the 95% CL fit. For these branching ratios we have set $\lambda_5 = \lambda_6 = \lambda_7 = 0$. Dependence of $\text{Br}(h \rightarrow hh)$ on the value of λ_5 is illustrated in Fig. 9 for $\lambda_6 = \lambda_7 = 0$. Note that when $\lambda_5 \neq 0$, $\Gamma(H \rightarrow hh)$ may be parametrically enhanced and further dominate over $\Gamma(H \rightarrow VV)$. For the pseudoscalar, Fig. 10 shows the production cross section times branching ratios of A as a function of m_A in Type 1 and Type 2 2HDM for the same two reference points; here there is no additional parametric freedom beyond the dependence on α and β .

Several features are immediately apparent, though these branching ratio plots are not necessarily generic. In Type 1 2HDM, away from the exact alignment limit the dominant modes for H are $H \rightarrow VV$, $H \rightarrow hh$, and $H \rightarrow t\bar{t}$. When kinematically available, the di-Higgs decay $H \rightarrow hh$ often dominates over $H \rightarrow VV$ due to $\mathcal{O}(1)$ numerical factors as well as $\tan\beta$ -enhancement away from the alignment limit. Whether or not $H \rightarrow t\bar{t}$ dominates the branching ratio when kinematically available depends on $\tan\beta$. Since y_{Htt} is suppressed at large $\tan\beta$ in a Type 1 2HDM, it may remain subdominant relative to $H \rightarrow hh$ provided sufficient distance from the alignment limit. Thus $H \rightarrow hh$ may remain the dominant decay mode of the non-SM-like heavy Higgs even when $m_H > 2m_t$. For A the dominant modes are $A \rightarrow b\bar{b}$, $A \rightarrow gg$, $A \rightarrow \tau^+\tau^-$, $A \rightarrow Zh$, and $A \rightarrow t\bar{t}$. When kinematically available, $A \rightarrow Zh$ dominates for $m_A < 2m_t$; when it becomes available, $A \rightarrow t\bar{t}$ may then dominate at low $\tan\beta$, but remains sub-dominant at high $\tan\beta$ due to the suppression of y_{Att} . Much like $H \rightarrow hh$, $A \rightarrow Zh$ may then remain the dominant decay mode even when $m_A > 2m_t$.

In Type 2 2HDM, the important modes are again $H \rightarrow VV$, $H \rightarrow hh$, $H \rightarrow t\bar{t}$ as well as $H \rightarrow \tau^+\tau^-$ and $H \rightarrow b\bar{b}$, both of which become important at large $\tan\beta$. In this case $H \rightarrow hh$ is rarely important once $m_H > 2m_t$, since either $H \rightarrow t\bar{t}$ takes over at low $\tan\beta$ or $H \rightarrow b\bar{b}$, $\tau^+\tau^-$ take over at high $\tan\beta$. For A the dominant modes are again $A \rightarrow b\bar{b}$, $A \rightarrow gg$, $A \rightarrow \tau^+\tau^-$, $A \rightarrow Zh$, and $A \rightarrow t\bar{t}$. When kinematically available, $A \rightarrow Zh$ dominates for $m_A < 2m_t$ at low $\tan\beta$ but is highly suppressed at high $\tan\beta$. Once it becomes kinematically available, $A \rightarrow t\bar{t}$ dominates at low $\tan\beta$, but is suppressed relative to $A \rightarrow b\bar{b}$ at high $\tan\beta$ due to the diminution of y_{Att} and enhancement of y_{Abb} .

In Type 3 2HDM, the parametric scaling is similar to Type 1 2HDM except at large $\tan\beta$, where eventually $H \rightarrow \tau^+\tau^-$ and $A \rightarrow \tau^+\tau^-$ take over the total widths. In Type 4 2HDM, the scaling is similar to Type 2 2HDM, except $H, A \rightarrow \tau^+\tau^-$ no longer play a role at

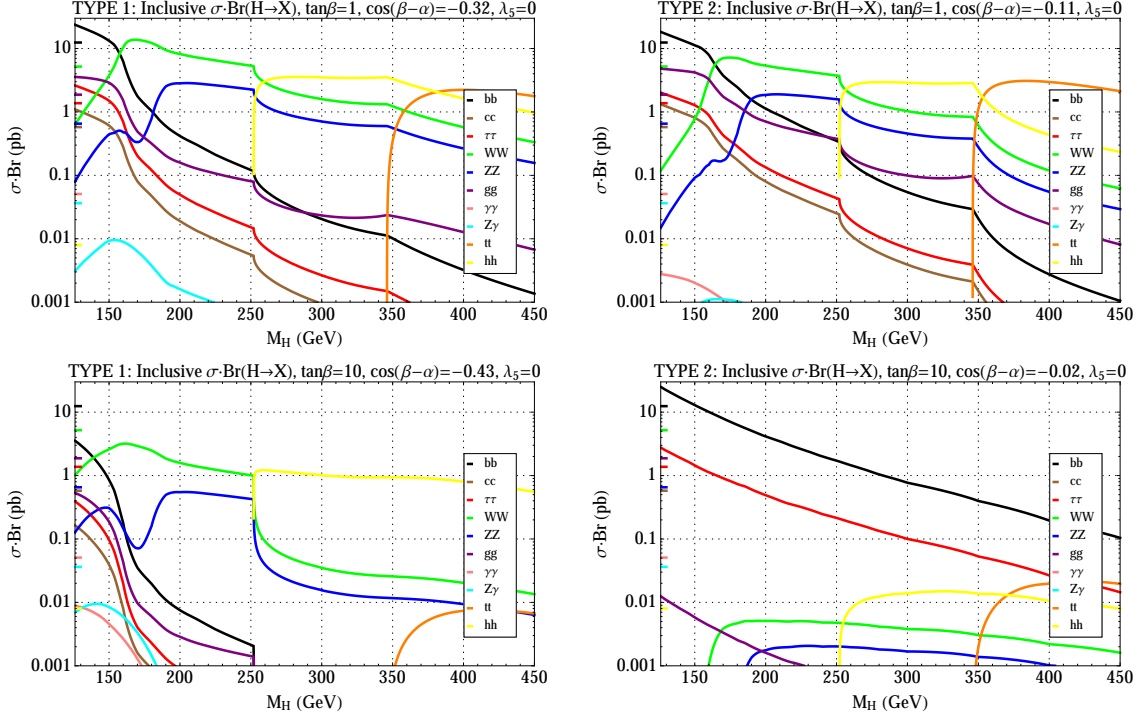


Figure 8. Cross section times branching ratio $\sigma \cdot \text{Br}(H \rightarrow X)$ to available final states in units of pb for 8 TeV pp collisions for the non-SM-like scalar Higgs boson, shown as a function of m_H . Upper left: $\tan \beta = 1$, $\cos(\beta - \alpha) = -0.32$ for Type 1 2HDM. Upper right: $\tan \beta = 1$, $\cos(\beta - \alpha) = -0.11$ for Type 2 2HDM. Lower left: $\tan \beta = 10$, $\cos(\beta - \alpha) = -0.43$ for Type 1 2HDM. Lower right: $\tan \beta = 10$, $\cos(\beta - \alpha) = -0.02$ for Type 2 2HDM. In each case we have chosen $\lambda_{5,6,7} = 0$ and $m_A = m_H$.

large $\tan \beta$.

Of course, the dominant modes in the branching ratios of H and A are not necessarily the best modes for discovery. In general the most fruitful standard channels (i.e., involving direct decays to SM final states) are those that may be distinguished above SM backgrounds, primarily:

- Inclusive production of H with $H \rightarrow VV^{(*)}$ or $H \rightarrow \gamma\gamma$
- Inclusive production of A with $A \rightarrow \gamma\gamma$
- Inclusive production of H or A with $H, A \rightarrow \tau^+\tau^-$ or $H, A \rightarrow \mu^+\mu^-$
- $t\bar{t}$ production with $t \rightarrow H^\pm \bar{b}$ and $H^\pm \rightarrow \tau^\pm \nu$

Beyond standard channels, it is useful to search for additional scalars through their decays to h and other states. Again assuming the approximate mass ordering $m_h < m_A \sim m_H \sim m_{H^\pm}$, the kinematically available channels with promising search prospects are:

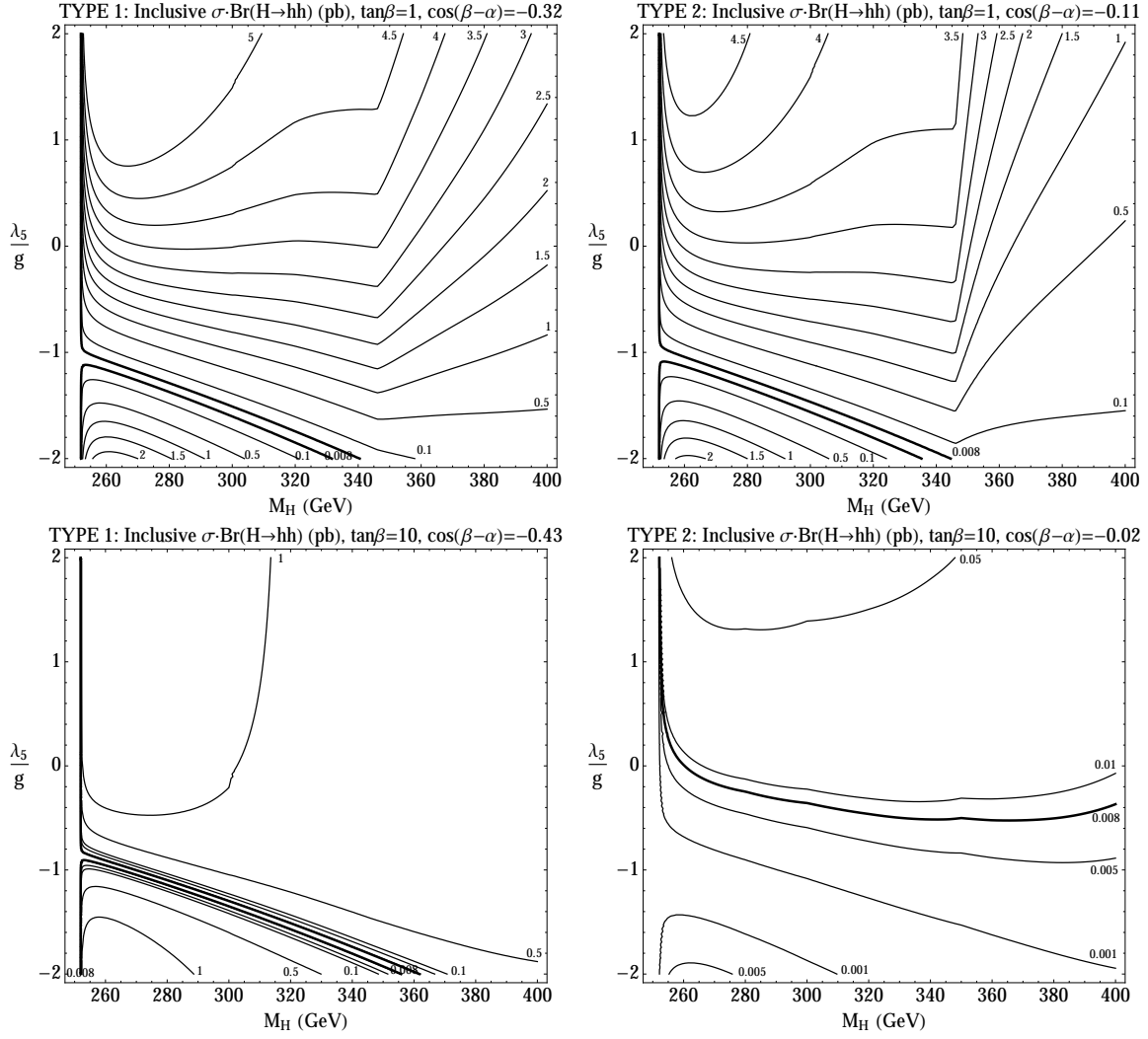


Figure 9. Contours of the inclusive $\sigma \cdot \text{Br}(H \rightarrow hh)$ in units of pb for 8 TeV pp collisions for the non-SM-like scalar Higgs boson, shown as a function of m_H and λ_5 . Upper left: $\tan\beta = 1$, $\cos(\beta - \alpha) = -0.32$ for Type 1 2HDM. Upper right: $\tan\beta = 1$, $\cos(\beta - \alpha) = -0.11$ for Type 2 2HDM. Lower left: $\tan\beta = 10$, $\cos(\beta - \alpha) = -0.43$ for Type 1 2HDM. Lower right: $\tan\beta = 10$, $\cos(\beta - \alpha) = -0.02$ for Type 2 2HDM. Here we have chosen $\lambda_{6,7} = 0$ and $m_A = m_H$.

- Inclusive production of H with $H \rightarrow hh$
- Inclusive production of A with $A \rightarrow Zh$
- $t\bar{b}$ associated production of H^\pm with $H^\pm \rightarrow W^\pm h$

Note the latter mode of $t\bar{b}$ associated production of H^\pm with $H^\pm \rightarrow W^\pm h$ is not kinematically available when $m_{H^\pm} < m_t$, and so the associated production cross section is bound to be

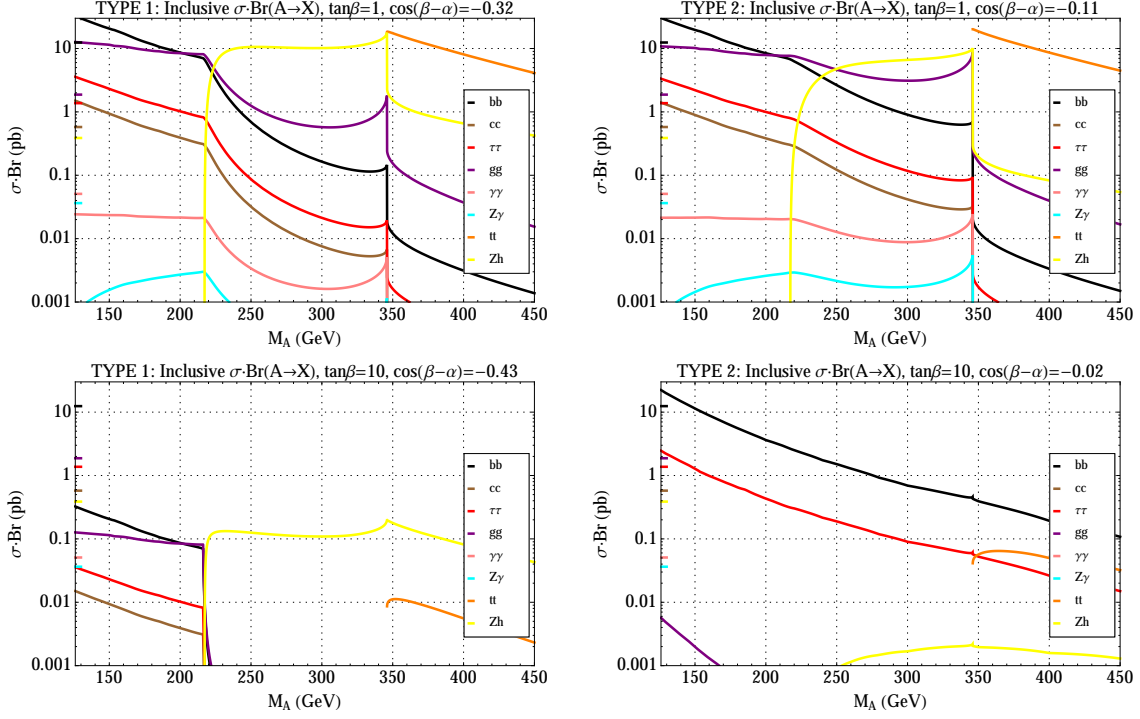


Figure 10. Cross section times branching ratio $\sigma \cdot \text{Br}(A \rightarrow X)$ to available final states in units of pb for 8 TeV pp collisions for the pseudoscalar Higgs boson, shown as a function of m_A . Upper left: $\tan \beta = 1$, $\cos(\beta - \alpha) = -0.32$ for Type 1 2HDM. Upper right: $\tan \beta = 1$, $\cos(\beta - \alpha) = -0.11$ for Type 2 2HDM. Lower left: $\tan \beta = 10$, $\cos(\beta - \alpha) = -0.43$ for Type 1 2HDM. Lower right: $\tan \beta = 10$, $\cos(\beta - \alpha) = -0.02$ for Type 2 2HDM. In each case we have chosen $\lambda_{5,6,7} = 0$ and $m_A = m_H$.

fairly small. We will not consider this case in detail here,⁷ but will instead focus on inclusive production of H and A with $H \rightarrow hh$ and $A \rightarrow Zh$, which may have sizable production cross sections and appreciable branching ratios.

While choosing benchmark values of α, β consistent with current signal fits and studying the branching ratios as a function of mass gives useful intuition, a more detailed study is required to understand the signals as α and β are varied. For simplicity, we focus on the benchmark mass $m_H = m_A = 300$ GeV where $H \rightarrow hh$ and $A \rightarrow Zh$ are kinematically available. The relative parametrics remain similar for $m_H < 2m_h$ and $m_A < m_Z + m_h$, save that the modes $H \rightarrow hh, A \rightarrow Zh$ are inaccessible and $H \rightarrow VV, A \rightarrow b\bar{b}$ become dominant. For $m_H, m_A > 2m_t$ the decays $H, A \rightarrow t\bar{t}$ become kinematically available, and may or may not dominate the total width depending on the 2HDM type and the value of $\tan \beta$.

As with the SM-like Higgs h , the parametric behavior of the production cross section times branching ratio for the processes of interest is governed by the scaling of the production mode, the decay mode, and the total width. For most of the cases we consider, production

⁷For a recent discussion of prospects for discovering $H^\pm \rightarrow W^\pm h$ at the LHC, see [59].

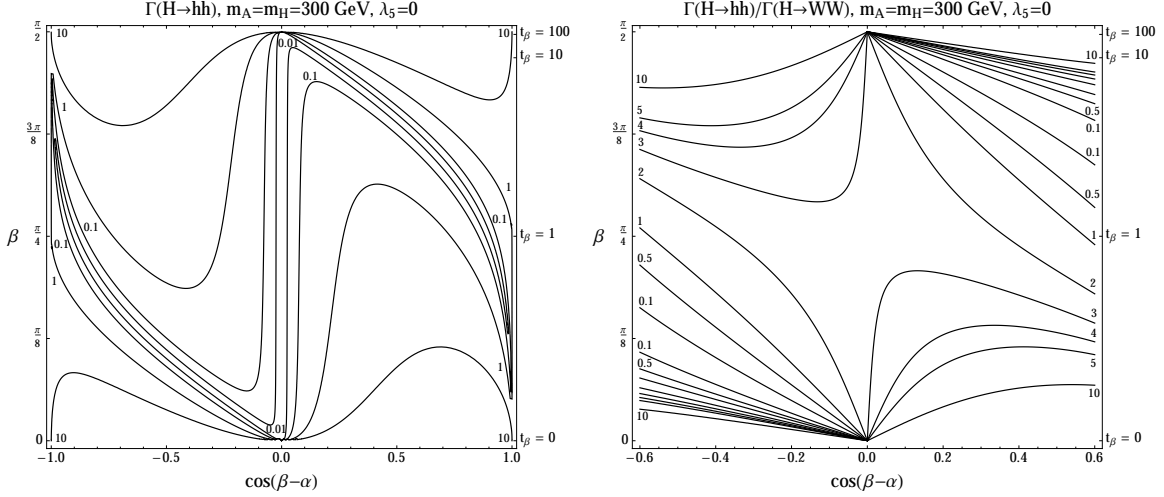


Figure 11. Left: Contours of $\Gamma(H \rightarrow hh)$ in units of pb for the non-SM-like scalar Higgs boson H in all four 2HDM types, shown as a function of $\cos(\beta - \alpha)$ and β . Right: Contours of $\Gamma(H \rightarrow hh)/\Gamma(H \rightarrow WW)$ for the non-SM-like scalar Higgs boson H in all four 2HDM types, shown as a function of $\cos(\beta - \alpha)$ and β . In both plots we have chosen $\lambda_{5,6,7} = 0$ and $m_A = m_H = 300$ GeV. The partial width $\Gamma(H \rightarrow hh)$ typically exceeds $\Gamma(H \rightarrow WW)$ over a wide range of parameter space.

is entirely dominated by gluon fusion and scales as $\sim y_{Htt}^2$. The only exception is in Type 2 and Type 4 2HDM at large $\tan\beta$, where $b\bar{b}H$ and $b\bar{b}A$ associated production take over and production scales as $\sim y_{Hbb}^2$ and $\sim y_{Abb}^2$, respectively.

On the decay side, the total width may vary considerably across the parameter space as different processes contribute in different regions. For the heavy CP even scalar H in a Type 1 2HDM, precisely in the alignment limit $H \rightarrow VV$ and $H \rightarrow hh$ vanish, leaving $h \rightarrow gg$ and $h \rightarrow b\bar{b}$ to constitute the bulk of the total width. For $m_H \gtrsim 2m_h$ the two widths are comparable, with $\Gamma(h \rightarrow gg) \gtrsim \Gamma(h \rightarrow b\bar{b})$ at $m_H = 300$ GeV. Thus in the strict alignment limit the total width scales as $\sim y_{Htt}^2 \sim y_{Hbb}^2$.

However, with even a small deviation from the alignment limit the partial widths for $H \rightarrow VV, hh$ rapidly come to dominate. Parametrically, the partial widths scale as

$$\frac{\Gamma(H \rightarrow WW, hh)}{\Gamma(H \rightarrow b\bar{b})} \propto \frac{g_{HVV}^2 m_H^2}{y_{Hbb}^2 m_b^2} \quad (6.1)$$

In a Type 1 2HDM, the ratio of coefficients scales as $\sim \cos^2(\beta - \alpha)$ around the alignment limit when $\tan\beta$ is not too large, which suggests that $H \rightarrow VV, hh$ take over the partial width when $|\cos(\beta - \alpha)| \gtrsim m_b/m_H \sim 0.02$. This turns out to be a good approximation; for $m_H = 300$ GeV, numerically we find $\Gamma(H \rightarrow WW) > \Gamma(H \rightarrow b\bar{b})$ for $|\cos(\beta - \alpha)| \gtrsim 0.03$ and $\tan\beta = 1$. The y_{Hbb} coupling is suppressed in Type 1 2HDM when $\tan\beta$ is large, so that $H \rightarrow VV, hh$ dominate even closer to the alignment limit in this case. Thus even very small deviations lead to $\Gamma(H \rightarrow VV)$ and $\Gamma(H \rightarrow hh)$ dominating the total width. Whether $H \rightarrow VV$ or $H \rightarrow hh$ dominates depends in detail on numerical coefficients; we see from Fig. 11 that it is typically

$\Gamma(H \rightarrow hh)$ that is greater by an $\mathcal{O}(1)$ numerical factor, with additional $\tan \beta$ enhancement away from the alignment limit. However, since g_{Hhh} also has additional zeroes away from the alignment limit, in these regions $\Gamma(H \rightarrow VV)$ takes over the total width.

For Type 2 2HDM the story is similar, except at large $\tan \beta$ where y_{Hbb} is $\tan \beta$ -enhanced and $H \rightarrow b\bar{b}$ takes over the partial width when $\lambda_{6,7} = 0$ (though as discussed above, when $\lambda_{6,7} \neq 0$ then g_{Hhh} is $\tan \beta$ -enhanced at leading order and continues to dominate the total width). This is again apparent from (6.1), which suggests that $\Gamma(h \rightarrow b\bar{b})$ dominates the partial width for $|\cos(\beta - \alpha)| \lesssim (m_b/m_H) \tan \beta$. Since current fits constrain $|\cos(\beta - \alpha)| \lesssim 0.1$ in Type 2 models, this suggests $H \rightarrow b\bar{b}$ dominates the total width as soon as $\tan \beta \gtrsim 5$. In practice, this is again a good approximation, and for $\cos(\beta - \alpha) = -0.1$ we find $\Gamma(H \rightarrow WW) \lesssim \Gamma(H \rightarrow b\bar{b})$ for $\tan \beta \gtrsim 3.6$.

For the pseudoscalar A , the competitive modes are $A \rightarrow Zh$, $A \rightarrow b\bar{b}$, and $A \rightarrow gg$. Parametrically, the partial widths scale as

$$\frac{\Gamma(A \rightarrow Zh)}{\Gamma(H \rightarrow b\bar{b})} \propto \frac{g_{AZh}^2}{y_{Abb}^2} \frac{m_A^2}{m_b^2} \quad (6.2)$$

In Type 1 2HDM, for moderate $\tan \beta$ we again have $\frac{g_{AZh}^2}{y_{Abb}^2} \propto \cos^2(\beta - \alpha)$ and expect $A \rightarrow Zh$ to dominate when $|\cos(\beta - \alpha)| \gtrsim m_b/m_A \sim 0.02$; numerically this is the case when $|\cos(\beta - \alpha)| \gtrsim m_b/m_A \sim 0.04$ for $\tan \beta = 1$, and $A \rightarrow Zh$ takes over even closer to the alignment limit when $\tan \beta$ is large. In Type 2 2HDM, the situation parallels the case for $H \rightarrow hh$; y_{Abb} is $\tan \beta$ -enhanced, and so $A \rightarrow b\bar{b}$ dominates when $\tan \beta \gtrsim 3$.

With this parametric understanding of the production and decay modes, it is straightforward to study the variation in potential signals of the scalars H and A as a function of α and β .

6.1 Inclusive production of H with $H \rightarrow VV^{(*)}$

Current searches for additional Higgs boson are primarily focused on $H \rightarrow VV^{(*)}$ at high mass. Although g_{HVV} is $\cos(\beta - \alpha)$ -suppressed around the alignment limit, since $\Gamma(H \rightarrow hh, VV^{(*)})$ comprise the majority of the total width this does not necessarily imply suppression of the branching ratio except very close to the exact alignment limit or, for Type 2 2HDM, at large $\tan \beta$ when $\Gamma(H \rightarrow b\bar{b})$ takes over. For $H \rightarrow VV$, we find it useful to illustrate the size of the available signal as a function of mass and $\tan \beta$, accounting for most of the α dependence by plotting contours of the inclusive $\sigma \cdot \text{Br}(H \rightarrow WW)/\cos^2(\beta - \alpha)$ as shown in Fig. 12. This illustrates how $\sigma \cdot \text{Br}(H \rightarrow WW)$ varies as a function of m_H , $\tan \beta$, and one may easily infer the value of $\sigma \cdot \text{Br}$ for any specific choice of $\cos(\beta - \alpha)$. Note that in general there is still weak dependence on α due to the variation of the total width, but Fig. 12 captures the leading parametric dependence. In both types of 2HDM, $\sigma \cdot \text{Br}(H \rightarrow WW)/\cos^2(\beta - \alpha)$ is suppressed at low m_H because one W boson is off-shell, and the rate rises rapidly when both W 's go on-shell. The rate falls at $m_H = 2m_h$ when $H \rightarrow hh$ becomes kinematically available, and likewise at $m_H = 2m_t$ when $H \rightarrow t\bar{t}$ opens. In Type 1 2HDM the rate falls

with increasing $\tan \beta$ simply because the production coupling y_{Htt} is $\tan \beta$ -suppressed, while in Type 2 2HDM the rate falls more rapidly because the production mode is suppressed and because the total width grows with $\tan \beta$ due to the enhancement of $\Gamma(H \rightarrow b\bar{b})$.

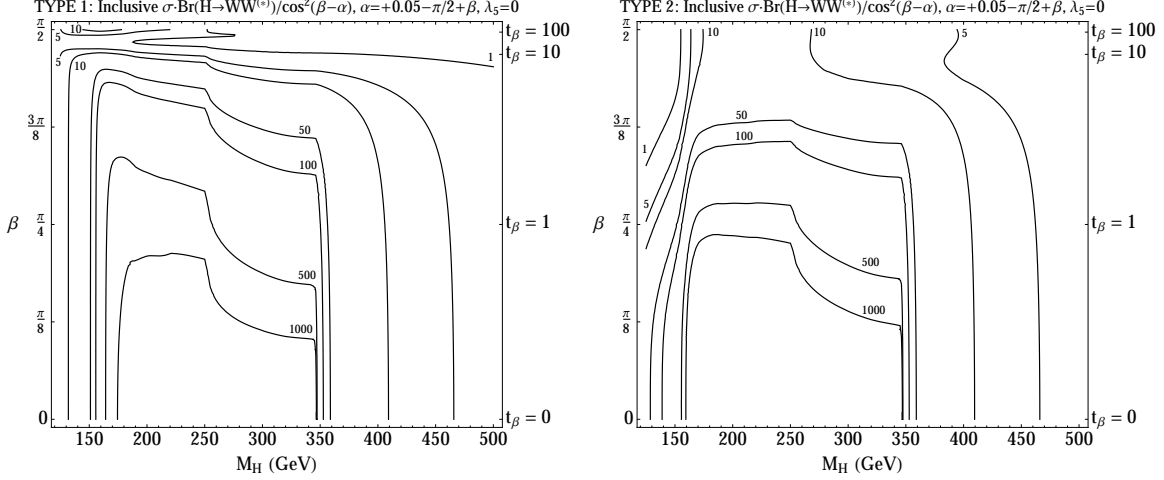


Figure 12. Contours of the inclusive $\sigma \cdot \text{Br}(H \rightarrow WW^{(*)})/\cos^2(\beta - \alpha)$ in units of pb for 8 TeV pp collisions for the non-SM-like scalar Higgs boson, shown as a function of m_H and β for Type 1 (left) and Type 2 (right) 2HDM. Here we have chosen $\alpha = 0.05 - \pi/2 + \beta$, $\lambda_{5,6,7} = 0$ and $m_A = m_H$.

Given that current LHC searches for additional Higgs scalars focus on the $H \rightarrow VV^{(*)}$ mode, it is also useful to consider the impact of present limits on the 2HDM parameter space. Fig. 13 illustrates the parametric variation of $\sigma \cdot \text{Br}(H \rightarrow VV^{(*)})$ as a function of α, β for the benchmark mass $m_H = 300$ GeV, normalized to the cross section times branching ratio of a SM-like Higgs of the same mass. Limits from current direct searches [60] for heavy SM-like Higgs bosons are also shown. Unsurprisingly, the rate depends primarily on $\tan \beta$ away from the alignment limit, since here $H \rightarrow hh, VV^{(*)}$ dominate the total width and the parametric dependence of the cross section times branching ratio comes from the production coupling y_{Htt} . In Type 2 2HDM the more rapid falloff at large $\tan \beta$ again arises because the total width grows with $\tan \beta$ due to the enhancement of $\Gamma(H \rightarrow b\bar{b})$. Very close to the alignment limit, $H \rightarrow b\bar{b}$ dominates the total width and $\text{Br}(H \rightarrow VV^{(*)})$ is diminished. For this particular benchmark with $\lambda_{5,6,7} = 0$, current searches exclude $\tan \beta \lesssim 2.5$ in both 2HDM types away from the alignment limit for $m_H = 300$ GeV. But note that this does not amount to an invariant bound, since if $\lambda_{5,6,7} \neq 0$ then the resulting increase in $\Gamma(H \rightarrow hh)$ further reduces $\text{Br}(H \rightarrow VV^{(*)})$ and softens the limit.

6.2 Inclusive production of H with $H \rightarrow \gamma\gamma$

Current searches for $H \rightarrow \gamma\gamma$ are truncated at relatively low mass, $m_H \sim 160$ GeV, since the already-small branching ratio for a SM-like Higgs falls rapidly with increasing mass. Nonetheless, $H \rightarrow \gamma\gamma$ may be important at high mass if the 2HDM is very close to the

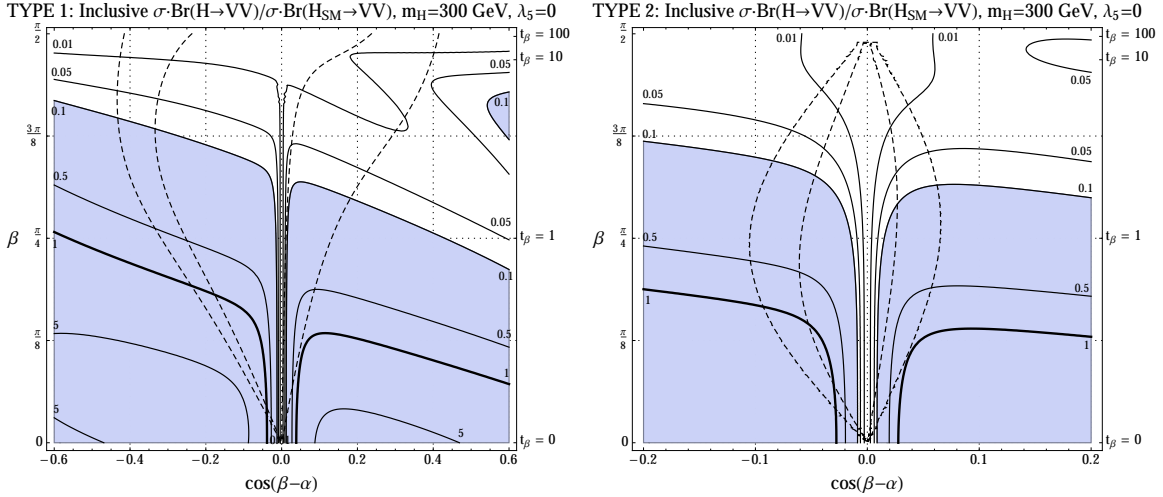


Figure 13. Contours of the inclusive $\sigma \cdot \text{Br}(H \rightarrow VV^{(*)})/\sigma \cdot \text{Br}(H_{SM} \rightarrow VV^{(*)})$ for 8 TeV pp collisions for the non-SM-like scalar Higgs boson, shown as a function of $\cos(\beta - \alpha)$ and β for Type 1 (left) and Type 2 (right) 2HDM. Here we have chosen $\lambda_{5,6,7} = 0$ and $m_A = m_H$. The inner (outer) dashed contour denotes the 68% (95%) CL best fit to the signals of the SM-like Higgs. The blue shaded region denotes the parameter space excluded by the most recent LHC searches for a heavy SM-like Higgs [60].

alignment limit, where the contributions from $H \rightarrow VV$ and $H \rightarrow hh$ vanish from the total width. Contours of the inclusive $\sigma \cdot \text{Br}(H \rightarrow \gamma\gamma)$ are shown in Fig. 14. For Type 1 2HDM, the rate falls with increasing $\tan\beta$ due to the $\tan\beta$ suppression of the production mode, while it peaks in the alignment limit because the total width drops precipitously as $H \rightarrow VV$ and $H \rightarrow hh$ decouple. The peaking is particularly sharp at large $\tan\beta$ because fermion partial widths are all suppressed by $\tan\beta$.

In Type 2 2HDM, the rate falls more rapidly with increasing $\tan\beta$ due to the suppressed production and the growing total width, though at large $\tan\beta$ the contributions from $b\bar{b}H$ associated production cause the rate to increase once again. The rate peaks in the alignment limit due to the decoupling of $H \rightarrow VV$ and $H \rightarrow hh$, but the peaking is less pronounced than in Type 1 2HDM because the non-decoupling contribution from $\Gamma(H \rightarrow b\bar{b})$ is always a fairly important contribution to the total width.

6.3 Inclusive production of A with $A \rightarrow \gamma\gamma$

Inclusive production of A with $A \rightarrow \gamma\gamma$ is entirely analogous to $H \rightarrow \gamma\gamma$ in its parametric scaling. Contours of the inclusive $\sigma \cdot \text{Br}(A \rightarrow \gamma\gamma)$ are shown in Fig. 15 and scale as discussed above, with slightly different modulation as the alignment limit is approached due to the fact that there is no contribution from W loops in the $A\gamma\gamma$ effective coupling.

In Fig. 16 we also illustrate the variation of the inclusive production of A with $A \rightarrow \gamma\gamma$ in the exact alignment limit as a function of mass and $\tan\beta$, focusing on low $\tan\beta$ where the rate is similar to the SM Higgs rate of ~ 51 fb at 8 TeV. In all 2HDM types, the rate falls

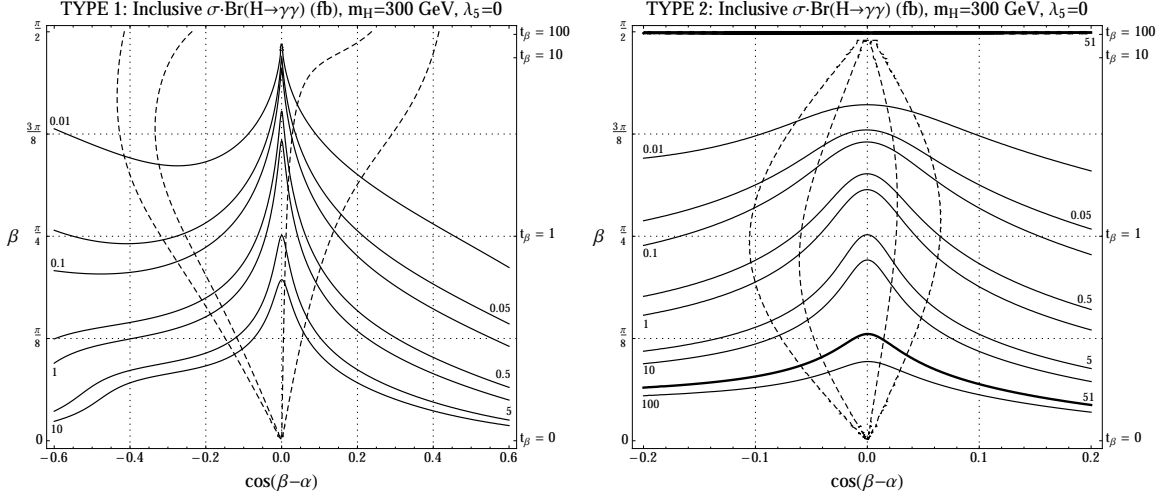


Figure 14. Contours of the inclusive $\sigma \cdot \text{Br}(H \rightarrow \gamma\gamma)$ in units of fb for 8 TeV pp collisions for the non-SM-like scalar Higgs boson with $m_H = 300$ GeV, shown as a function of $\cos(\beta - \alpha)$ and β for Type 1 (left) and Type 2 (right) 2HDM. Here we have chosen $\lambda_{5,6,7} = 0$ and $m_A = m_H$. The inner (outer) dashed contour denotes the 68% (95%) CL best fit to the signals of the SM-like Higgs.

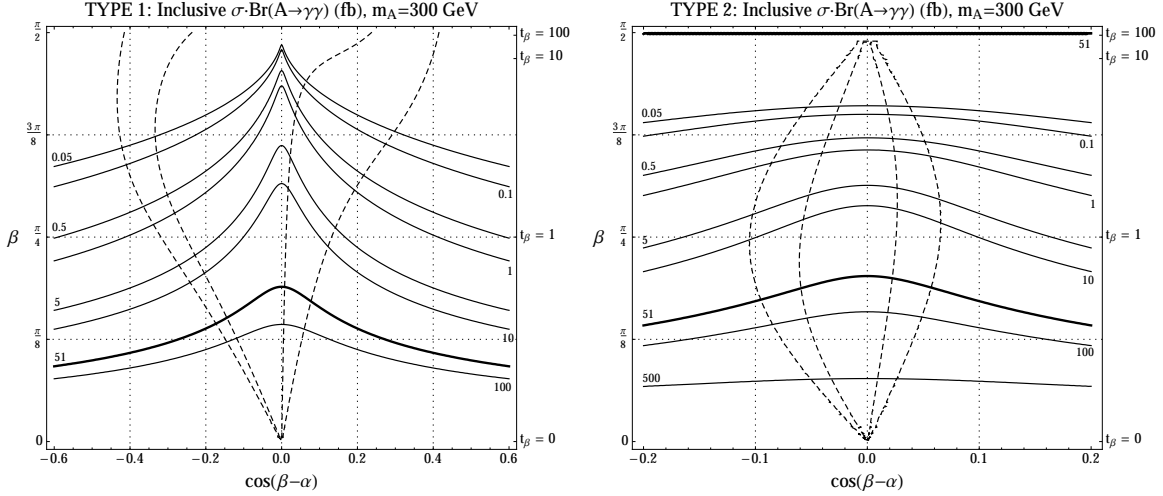


Figure 15. Contours of the inclusive $\sigma \cdot \text{Br}(A \rightarrow \gamma\gamma)$ in units of fb for 8 TeV pp collisions for the pseudoscalar Higgs boson with $m_A = 300$ GeV, shown as a function of $\cos(\beta - \alpha)$ and β for Type 1 (left) and Type 2 (right) 2HDM. The inner (outer) dashed contour denotes the 68% (95%) CL best fit to the signals of the SM-like Higgs.

rapidly with $\tan \beta$ due to the diminution of the y_{Att} coupling. In Type 2 and Type 4 2HDM the inclusive rate rises again at large $\tan \beta$ due to $b\bar{b}A$ associated production, but not to the extent that the rate again reaches SM Higgs-like values. In all cases, once $m_A > 2m_t$ the increase in total width due to $A \rightarrow t\bar{t}$ rapidly diminishes $\text{Br}(A \rightarrow \gamma\gamma)$.

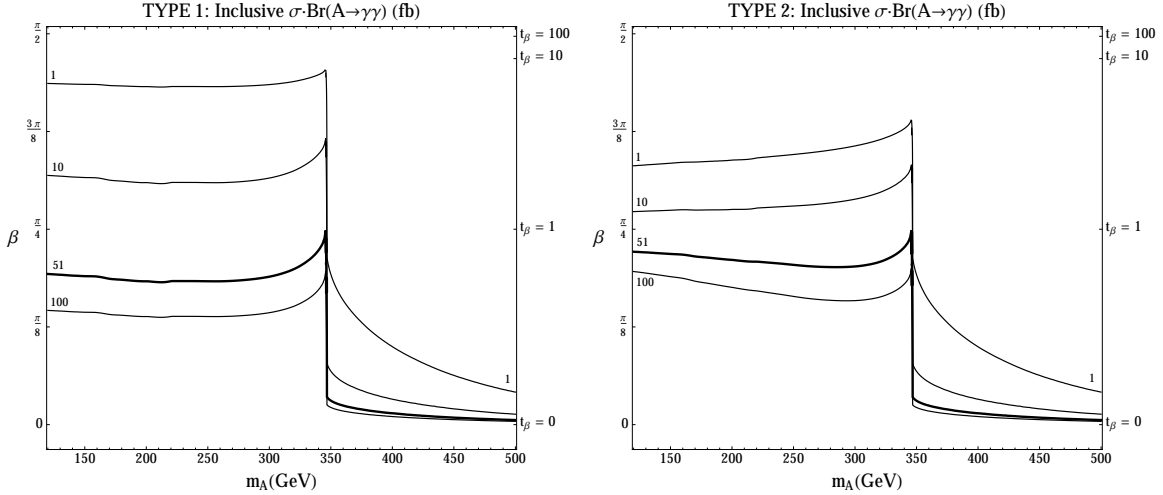


Figure 16. Contours of the inclusive $\sigma \cdot \text{Br}(A \rightarrow \gamma\gamma)$ in units of fb for 8 TeV pp collisions for the pseudoscalar Higgs boson in the exact alignment limit, shown as a function of m_A and $\tan\beta$ for Type 1 (left) and Type 2 (right) 2HDM. The thick line denotes the rate for a SM Higgs at 126 GeV of ~ 51 fb at 8 TeV pp collisions.

6.4 Inclusive production of H or A with $H, A \rightarrow \tau^+\tau^-$ or $H, A \rightarrow \mu^+\mu^-$

Inclusive production of H or A with $H, A \rightarrow \tau^+\tau^-$ plays a particularly important role in searches for MSSM-like 2HDM, since $\Gamma(H \rightarrow \tau^+\tau^-)$ is $\tan\beta$ -enhanced. As such, high-mass searches for new scalars decaying to taus are already conducted at both ATLAS and CMS. Here we illustrate the parametric scaling as a function of m_H, m_A and $\tan\beta$ in the exact alignment limit, $\sin(\beta - \alpha) = 1$, where this mode is expected to play a particularly strong role in discovery of new scalars. If both H and A are similar in mass, the poor mass resolution in the di-tau final state makes it useful to exhibit the collective signal from both states. Contours of the inclusive $\sigma \cdot \text{Br}(A \rightarrow \tau^+\tau^-) + \sigma \cdot \text{Br}(H \rightarrow \tau^+\tau^-)$ are shown in Fig. 17.

In Type 1 2HDM, the rate is particularly small, falling with $\tan\beta$ due to the suppression of the gluon fusion production mode and disappearing entirely once $H, A \rightarrow t\bar{t}$ becomes kinematically accessible.

In Type 2 2HDM the prospects are much greater due to the $\tan\beta$ enhancement of $\Gamma(H \rightarrow \tau^+\tau^-)$. Features at low $\tan\beta$ are due to the interplay of the production modes. As $\tan\beta$ increases, gluon fusion is suppressed due to the falling y_{Htt}, y_{Att} couplings, while $b\bar{b}H$ and $b\bar{b}A$ associated production is enhanced. The crossover takes place around $\tan\beta \sim 5$. The features around $m_H \sim 2m_t$ are a result of the interplay between the production mode crossover and the emergence of the two-top threshold.

Note that the parametric dependence for inclusive production of H or A with $H, A \rightarrow \mu^+\mu^-$ is identical; the rate may be obtained from that of $H, A \rightarrow \tau^+\tau^-$ by simply rescaling with a factor of $m_\mu^2/m_\tau^2 \sim 0.0035$. Needless to say, this results in a vanishingly small rate for Type 1 2HDM, but a multi-fb rate for Type 2 2HDM. Searches in this channel are attractive

due to the considerable mass resolution available in the di-muon final state. Given the important role of leptonic decays of H and A in the alignment limit, it is important to perform searches for resonant di-muon production out to high masses.

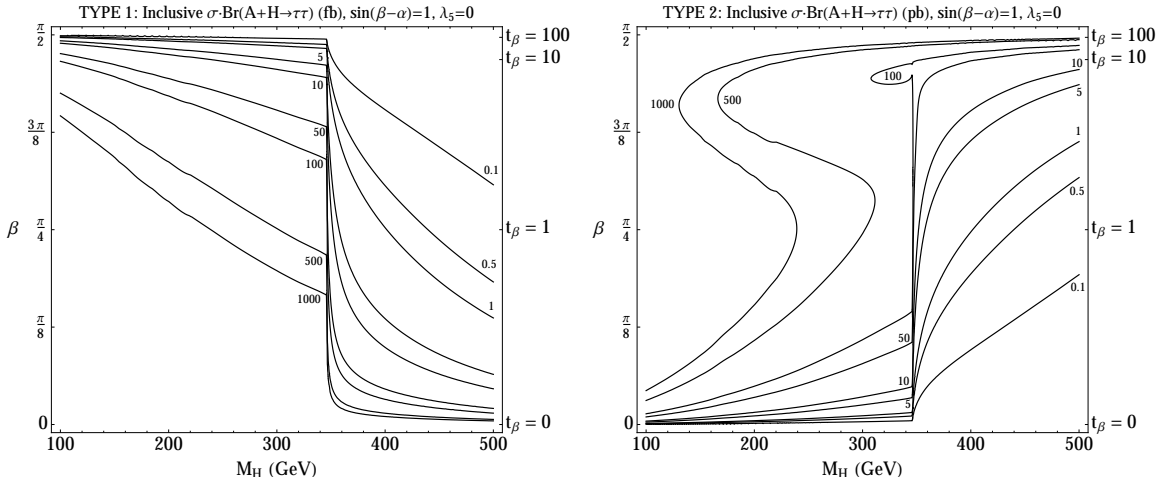


Figure 17. Contours of the inclusive $\sigma \cdot \text{Br}(A \rightarrow \tau^+ \tau^-) + \sigma \cdot \text{Br}(A \rightarrow \tau^+ \tau^-)$ for 8 TeV pp collisions for the sum of pseudoscalar and non-SM-like scalar Higgs bosons in the alignment limit $\sin(\beta - \alpha) = 1$, shown as a function of m_H and $\tan \beta$ in units of fb for Type 1 (left) and in units of pb for Type 2 (right) 2HDM. Here we have chosen $\lambda_{5,6,7} = 0$.

6.5 Inclusive production with $H \rightarrow hh$

Perhaps the most striking signal for the discovery of a heavy CP-even neutral Higgs is inclusive production of H followed by $H \rightarrow hh$. As discussed earlier, this process often dominates the total width when kinematically available, and may even remain the largest branching ratio for $m_H > 2m_t$ in Type 1 2HDM at large $\tan \beta$. The process leads to a variety of distinctive final states and the production cross section times branching ratio greatly exceeds the SM expectation of ~ 8 fb at 8 TeV.

Contours of the inclusive $\sigma \cdot \text{Br}(H \rightarrow hh)$ are shown in Fig. 18 for $\lambda_{5,6,7} = 0$. For Type 1 2HDM, the production mode is dominated by gluon fusion and the decay mode is parametrically identical to the total width except where $g_{Hhh} \rightarrow 0$. Thus the parametrics are governed by three features: (1) the falling production rate at large $\tan \beta$ due to diminishing y_{Htt} ; (2) the vanishing of g_{Hhh} in the alignment limit; and (3) the zeroes of g_{Hhh} associated with $\cos(2\beta - 2\alpha) - \frac{\sin(2\beta - 2\alpha)}{\tan(2\beta)} \approx \frac{1}{2} \frac{1}{1 - m_h^2/m_H^2}$. The zero for $\cos(\beta - \alpha) > 0$ approximately coincides with the zero in y_{Htt} , leading to the broad region of diminution around $\alpha \approx 0$.

For Type 2 2HDM, the production mode is dominated by gluon fusion except at large $\tan \beta$ where $b\bar{b}H$ associated production takes over. The decay mode is parametrically identical to the total width at low $\tan \beta$ except in the exact alignment limit, while at high $\tan \beta$ the total width scales with $y_{Hbb}^2 \propto \tan^2 \beta$. Thus the features are again governed by the falling

gluon fusion production rate at large $\tan\beta$ – exacerbated by the growing width – and the zeros of g_{Hhh} .

In both cases, it bears emphasizing that $\sigma \cdot \text{Br}(H \rightarrow hh)$ may be quite large – more than a picobarn, two orders of magnitude larger than the SM rate – while remaining consistent with current coupling fits to the signals of h . Even when $\lambda_{5,6,7} = 0$ the rate may remain high in light of direct limits on $H \rightarrow VV$, and nonzero $\lambda_{5,6,7}$ have the dual effect of increasing $\sigma \cdot \text{Br}(H \rightarrow hh)$ and weakening direct limits on $H \rightarrow VV$ by lowering $\sigma \cdot \text{Br}(H \rightarrow VV)$.

Note in particular that for Type 1 2HDM, the region with enhanced VBF production of h with $h \rightarrow \gamma\gamma, VV^*$ corresponds to $\sigma \cdot \text{Br}(H \rightarrow hh) \gtrsim 1$ pb. This implies that if VBF production remains high due to Type 1 couplings, there is a large and readily discoverable rate for $\sigma \cdot \text{Br}(H \rightarrow hh)$ if H is not too heavy.

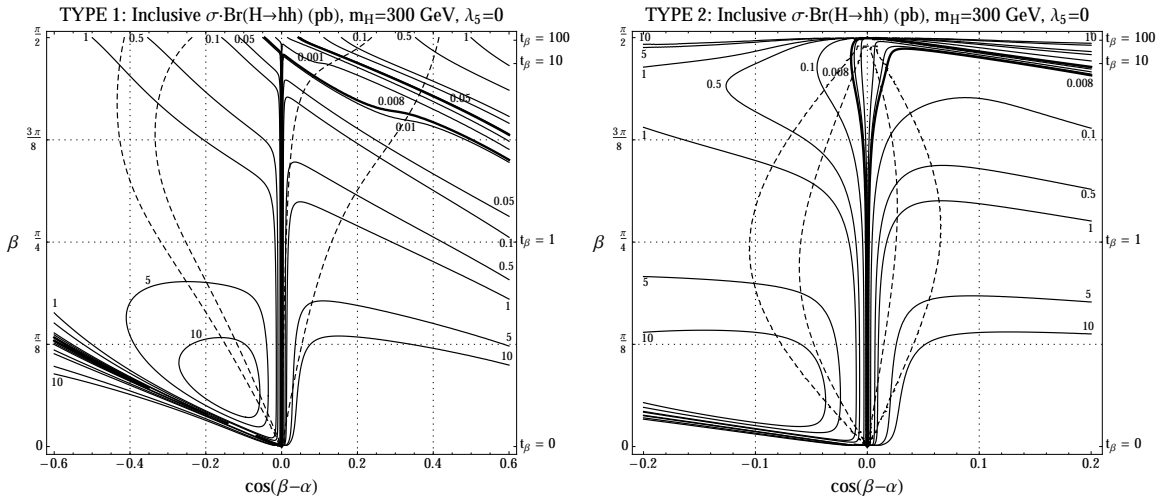


Figure 18. Contours of the inclusive $\sigma \cdot \text{Br}(H \rightarrow hh)$ in units of pb for 8 TeV pp collisions for the non-SM-like scalar Higgs boson with $m_H = 300$ GeV, shown as a function of $\cos(\beta - \alpha)$ and β for Type 1 (left) and Type 2 (right) 2HDM. Here we have chosen $\lambda_{5,6,7} = 0$ and $m_A = m_H$. The inner (outer) dashed contour denotes the 68% (95%) CL best fit to the signals of the SM-like Higgs.

Contours of the inclusive $\sigma \cdot \text{Br}(H \rightarrow hh)$ are shown in Fig. 19 for $\lambda_5 = 0$ and $\lambda_{6,7}v^2 = (300 \text{ GeV})^2$. When $\lambda_{6,7}$ are nonzero, the $\tan\beta$ -enhanced contributions to $\Gamma(H \rightarrow hh)$ ensure that it comprises an even larger component of the total width and dominates even at large $\tan\beta$ in Type 2 2HDM.

6.6 Inclusive production with $A \rightarrow Zh$

Inclusive production of the pseudoscalar A with $A \rightarrow Zh$ plays a role quite analogous to inclusive production of H with $H \rightarrow hh$, often governing the total width when kinematically available and potentially providing one of the most promising modes for discovery of additional scalars at the LHC. Although there are Zh associated production searches at both ATLAS and CMS, which place a constraint on excessive enhancement of the total Zh cross section,

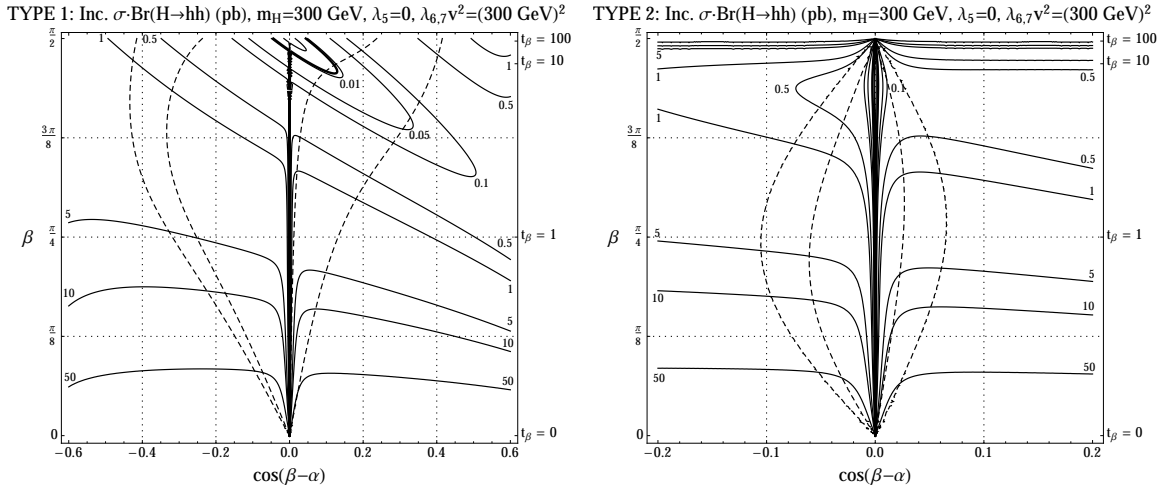


Figure 19. Contours of the inclusive $\sigma \cdot \text{Br}(H \rightarrow hh)$ in units of pb for 8 TeV pp collisions for the non-SM-like scalar Higgs boson with $m_H = 300$ GeV, shown as a function of $\cos(\beta - \alpha)$ and β for Type 1 (left) and Type 2 (right) 2HDM. Here we have chosen $\lambda_5 = 0$, $\lambda_{6,7}v^2 = (300 \text{ GeV})^2$, and $m_A = m_H$. The inner (outer) dashed contour denotes the 68% (95%) CL best fit to the signals of the SM-like Higgs.

sensitivity may be improved significantly by searching for resonant production of the Zh final state.

Contours of the inclusive $\sigma \cdot \text{Br}(A \rightarrow Zh)$ are shown in Fig. 20. The parametric scaling is relatively straightforward. In Type 1 2HDM the production mode is primarily gluon fusion, and so falls with y_{Att} at large $\tan \beta$, while the decay mode vanishes only in the exact alignment limit and otherwise controls the total width. Near the alignment limit, it is particularly dominant at large $\tan \beta$ where the fermion partial widths are $\tan \beta$ -suppressed. This combination of features entirely explains the distinctive shape of the $\sigma \cdot \text{Br}(A \rightarrow Zh)$ contours in Type 1 2HDM.

In Type 2 2HDM, the story is entirely analogous at low $\tan \beta$. At high $\tan \beta$, $b\bar{b}A$ associated production increases the production rate, but the total width is increasingly controlled by $\Gamma(A \rightarrow b\bar{b})$. This explains the broadening of contours at large $\tan \beta$ relative to the Type 1 case.

Much as with $H \rightarrow hh$, for Type 1 2HDM, the region with enhanced VBF production of h with $h \rightarrow \gamma\gamma, VV^*$ corresponds to $\sigma \cdot \text{Br}(A \rightarrow Zh) \gtrsim 1$ pb. Again, if VBF production remains high due to Type 1 couplings, there is a large and discoverable rate for $\sigma \cdot \text{Br}(A \rightarrow Zh)$ if A is not too heavy.

6.7 $t\bar{t}$ production with $t \rightarrow H^\pm \bar{b}$ and $H^\pm \rightarrow \tau^\pm \nu$

The inclusive production cross section for H^\pm is generally quite small, coming primarily from $t\bar{t}H^\pm$ associated production, but the rate may be appreciable when $m_{H^\pm} < m_t$ and H^\pm appears as a rare decay mode in $t\bar{t}$ pair production. As with di-tau production, searches for

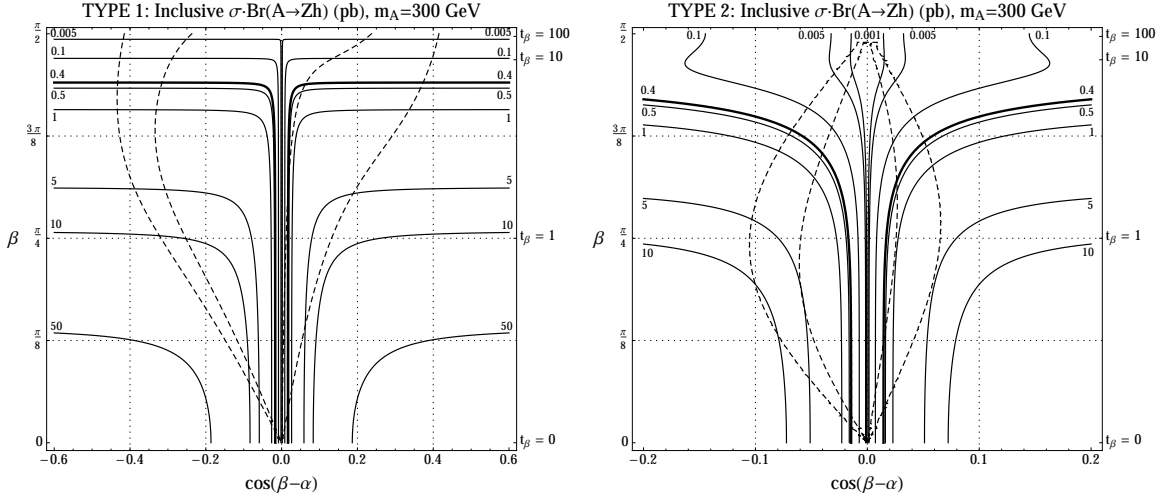


Figure 20. Contours of the inclusive $\sigma \cdot \text{Br}(A \rightarrow Zh)$ in units of pb for 8 TeV pp collisions for the pseudoscalar Higgs boson with $m_A = 300$ GeV, shown as a function of $\cos(\beta - \alpha)$ and β for Type 1 (left) and Type 2 (right) 2HDM. The inner (outer) dashed contour denotes the 68% (95%) CL best fit to the signals of the SM-like Higgs.

$t\bar{t}$ production with $t \rightarrow H^\pm \bar{b}$ and $H^\pm \rightarrow \tau^\pm \nu$ are already carried out in the context of MSSM-like 2HDM, but we reproduce the parametrics here for both Type 1 and Type 2 2HDM for completeness.

Contours of the combined branching ratio $\text{Br}(t \rightarrow H^\pm \bar{b}) \cdot \text{Br}(H^\pm \rightarrow \tau^\pm \nu)$ are shown in Fig. 21. For $m_{H^\pm} < m_t$, $\Gamma(H^\pm \rightarrow \tau^\pm \nu)$ uniformly dominates the total width. The contours are governed largely by $\Gamma(t \rightarrow H^\pm \bar{b})$, which accumulates contributions proportional to both y_{Att} and y_{Abb} . Thus in Type 1 2HDM the branching ratio falls with both $\tan \beta$ and mass as the fermion couplings and phase space are suppressed. In Type 2 2HDM, contributions due to y_{Att} are important at low $\tan \beta$, and transition to contributions from y_{Abb} at large $\tan \beta$, all modulated by the decreasing phase space as m_{H^\pm} is increased.

6.8 Signals of degenerate Higgses

Finally, it is interesting to consider the possibility that the observed signals at 126 GeV could arise from two near-degenerate scalars, which if sufficiently degenerate could not be distinguished with current experimental resolution. The inclusive contributions from H or A degenerate with h are shown in Figs. 22 and 23, respectively. We also show the VBF contribution from H degenerate with h in Fig. 24. We do not overlay fits to the current Higgs signal, since the fits were performed under the hypothesis that only h contributes.⁸ Unsurprisingly, near the alignment limit, the signal typically exceeds that of the SM Higgs,

⁸Performing a fit to signals originating from degenerate h and H/A would in any event require accurately accounting for the possibility of large production in association with b quarks due to β -dependent couplings that can enhance this mode. This is however not a production mode for which experimental efficiencies are presently known, so assuming such a signal would necessarily jeopardize the credibility of such fits.

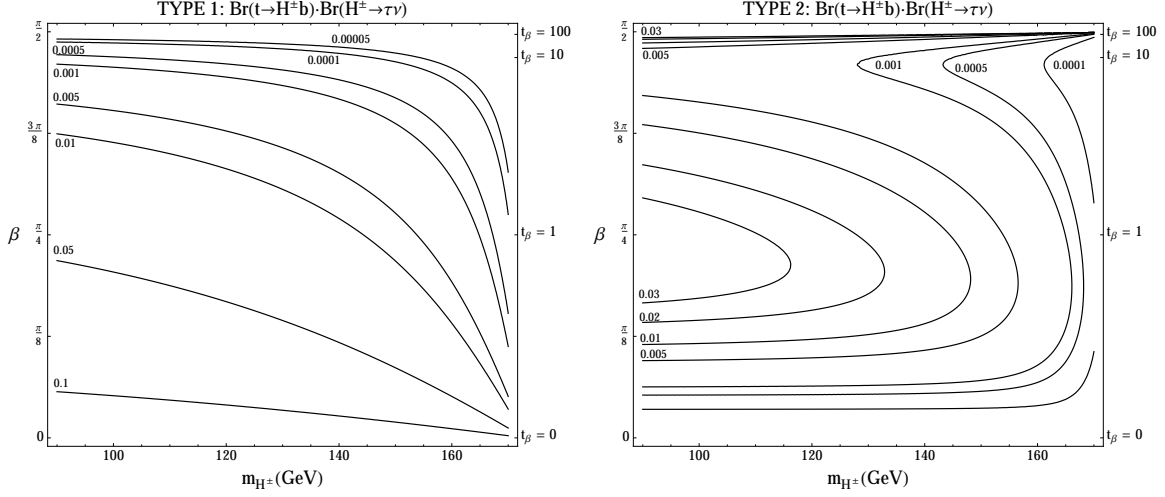


Figure 21. Contours of the combined branching ratio $\text{Br}(t \rightarrow H^\pm b) \cdot \text{Br}(H^\pm \rightarrow \tau^\pm \nu)$, shown as a function of m_H and $\tan\beta$ for Type 1 (left) and Type 2 (right) 2HDM.

since the additional contributions from H or A are maximized in the alignment limit. In practice, distinguishing such degenerate Higgses is experimentally challenging given the limited mass resolution at the LHC, but there is some potential to resolve degenerate states using appropriate cross-ratios of branching ratios [61].

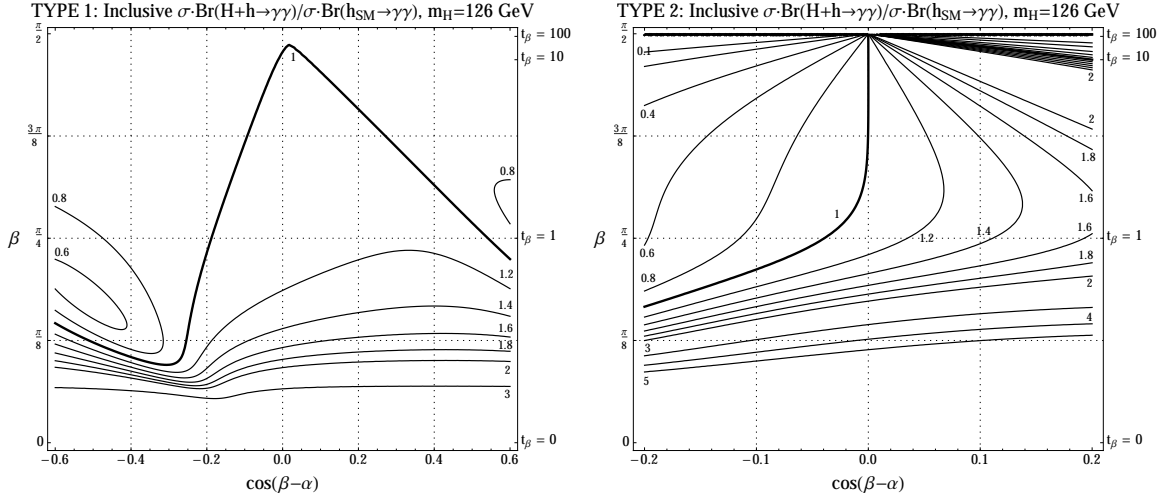


Figure 22. Contours of the inclusive $\sigma \cdot \text{Br}(H+h \rightarrow \gamma\gamma) / \sigma \cdot \text{Br}(h_{SM} \rightarrow \gamma\gamma)$ for 8 TeV pp collisions for the sum of contributions from the SM-like and non-SM-like scalar Higgs bosons with $m_H = m_h = 126$ GeV, shown as a function of $\cos(\beta - \alpha)$ and β for Type 1 (left) and Type 2 (right) 2HDM.

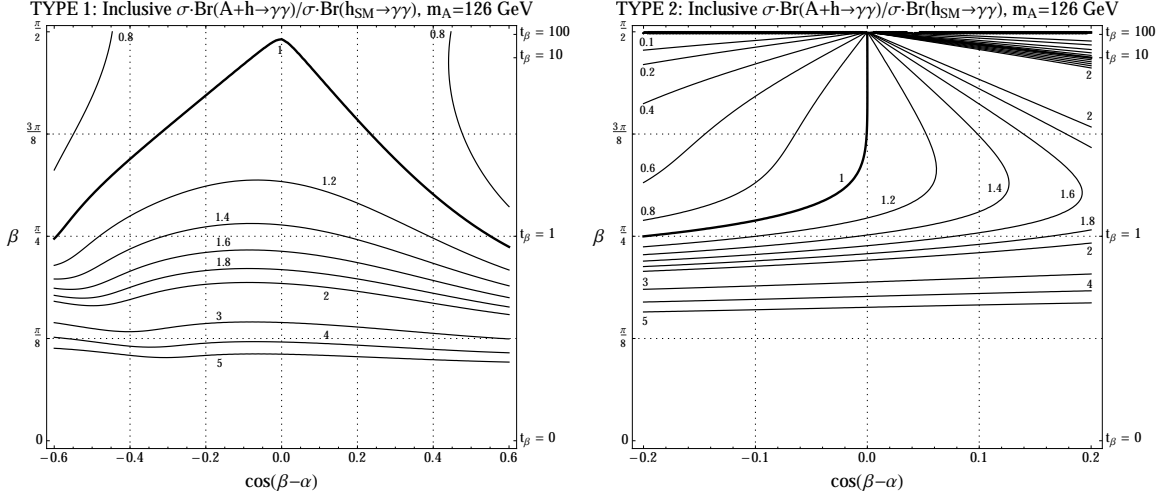


Figure 23. Contours of the inclusive $\sigma \cdot \text{Br}(A+h \rightarrow \gamma\gamma)/\sigma \cdot \text{Br}(h_{SM} \rightarrow \gamma\gamma)$ for 8 TeV pp collisions for the sum of contributions from the SM-like and pseudoscalar Higgs bosons with $m_A = m_h = 126$ GeV, shown as a function of $\cos(\beta - \alpha)$ and β for Type 1 (left) and Type 2 (right) 2HDM.

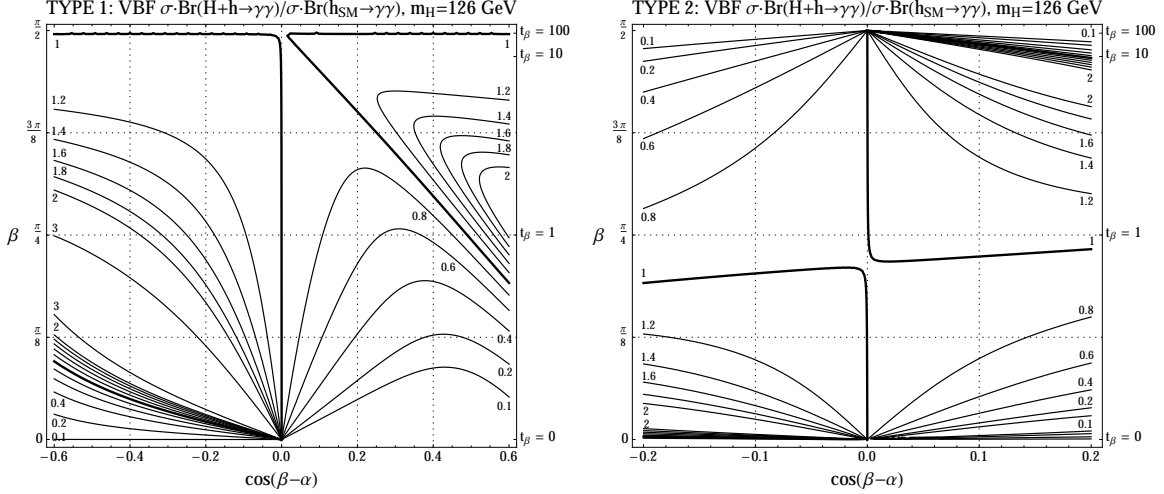


Figure 24. Contours of the VBF $\sigma \cdot \text{Br}(H+h \rightarrow \gamma\gamma)/\sigma \cdot \text{Br}(h_{SM} \rightarrow \gamma\gamma)$ for 8 TeV pp collisions for the sum of contributions from the SM-like and non-SM-like scalar Higgs bosons with $m_H = m_h = 126$ GeV, shown as a function of $\cos(\beta - \alpha)$ and β for Type 1 (left) and Type 2 (right) 2HDM.

7 Conclusions

The search for the Higgs at the LHC is entering a new post-discovery phase in which measurements of the SM-like Higgs couplings and direct searches for additional scalars begin to explore the parameter space of extended electroweak symmetry breaking sectors. In this work we have constructed a map between current signal fits to the SM-like Higgs, potential deviations in future measurements of the SM-like Higgs, and possible signals of additional

Higgs scalars in the context of theories with two Higgs doublets. Our work highlights a number of important observations that should be incorporated into LHC searches for additional Higgs scalars. Coupling measurements of the SM-like Higgs suggest that, in the context of 2HDM, the most promising channels for discrepancies in future measurements include VBF and Vh production of h with $h \rightarrow \gamma\gamma$ or $h \rightarrow VV^*$ as well as inclusive production of h with $h \rightarrow \tau^+\tau^-$, all of which are correlated and may be enhanced by as much as 80% (20%) above SM predictions consistent with current fits for case of a Type 1 (Type 2) 2HDM.

Coupling measurements of the SM-like Higgs also constrain the production modes for heavier Higgses. Away from the alignment limit, the gluon fusion production of H with decay to hh (when kinematically available) may exceed the SM rate for Higgs pair production by more than two orders of magnitude consistent with current coupling fits. This process may dominate decays of H even when $m_H > 2m_t$, providing a promising search channel for high-mass Higgs bosons. It may also reduce the branching ratio of H to vector bosons, weakening limits from current direct searches for $H \rightarrow VV$. Similarly, gluon fusion production of A with decay to Zh may be more than twice the SM rate for Zh associated production. These rates remain appreciable close to the alignment limit since both $\Gamma(H \rightarrow hh)$ and $\Gamma(A \rightarrow Zh)$ scale as $\propto m^3/v^2$, compensating somewhat for alignment limit-suppression. Very close to the alignment limit these modes become subdominant, but gluon fusion production of H, A with decay to $\gamma\gamma, \tau^+\tau^-$, and $\mu^+\mu^-$ may all be appreciable and provide promising avenues for discovering additional scalars even if the light Higgs is completely SM-like.

Our results suggest that $H \rightarrow hh$ and $A \rightarrow Zh$ should become high priorities in searching for additional Higgs bosons. The possibility of observable signals in $\gamma\gamma, \tau^+\tau^-$, and $\mu^+\mu^-$ final states in the exact alignment limit suggest these searches should be extended to higher Higgs masses.

Note Added: While this manuscript was being completed, [62–64] appeared, addressing aspects of the interplay between coupling fits and additional signals in certain 2HDM types.

Acknowledgments

We thank Kyle Cranmer, Sally Dawson, Aleandro Nisati, and Marc Sher for useful discussions. NC and ST are supported in part by the DOE under grant DE-FG02-96ER40959. NC is also supported by the NSF under grant PHY-0907744 and the Institute for Advanced Study. The work of J.G. is supported by the ERC Advanced Grant No. 267985 *Electroweak Symmetry Breaking, Flavour and Dark Matter: One Solution for Three Mysteries (DaMeSyFla)*.

A Hhh Coupling

The magnitudes of 2HDM couplings that involve more than two Higgs boson scalars depend in detail on the underlying interactions. For definiteness we consider here renormalizable

models with general CP-conserving tree-level potential

$$\begin{aligned}
V = & m_{11}^2 \Phi_1^\dagger \Phi_1 + m_{22}^2 \Phi_2^\dagger \Phi_2 - \left[m_{12}^2 \Phi_1^\dagger \Phi_2 + \text{h.c.} \right] \\
& + \frac{1}{2} \lambda_1 (\Phi_1^\dagger \Phi_1)^2 + \frac{1}{2} \lambda_2 (\Phi_2^\dagger \Phi_2)^2 + \lambda_3 (\Phi_1^\dagger \Phi_1) (\Phi_2^\dagger \Phi_2) + \lambda_4 (\Phi_1^\dagger \Phi_2) (\Phi_2^\dagger \Phi_1) \\
& + \left[\frac{1}{2} \lambda_5 (\Phi_1^\dagger \Phi_2)^2 + \lambda_6 (\Phi_1^\dagger \Phi_1) (\Phi_1^\dagger \Phi_2) + \lambda_7 (\Phi_2^\dagger \Phi_2) \Phi_1^\dagger \Phi_2 + \text{h.c.} \right]
\end{aligned} \tag{A.1}$$

The Feynman diagram coupling for Hhh with $SU(2)_L \times U(1)_Y \rightarrow U(1)_Q$ electroweak symmetry breaking may be obtained from the quartic interactions in (A.2) by eliminating the fields Φ_1^0 and Φ_2^0 in favor of the mass eigenstates h and H and expectation values v_1 and v_2 using the mixing relations (2.3) with the result

$$\begin{aligned}
g_{Hhh} = & \frac{v}{4} \left[\cos \alpha \left(- (3\lambda_1 + \lambda_3 + \lambda_4 + \lambda_5) \cos \beta - 3(\lambda_6 + \lambda_7) \sin \beta \right) \right. \\
& + \sin \alpha \left(- (3\lambda_2 + \lambda_3 + \lambda_4 + \lambda_5) \sin \beta - 3(\lambda_6 + \lambda_7) \cos \beta \right) \\
& + 3 \cos(3\alpha) \left((\lambda_1 - \lambda_3 - \lambda_4 - \lambda_5) \cos \beta + (\lambda_6 - 3\lambda_7) \sin \beta \right) \\
& \left. + 3 \sin(3\alpha) \left((-\lambda_2 + \lambda_3 + \lambda_4 + \lambda_5) \sin \beta + (3\lambda_6 - \lambda_7) \cos \beta \right) \right]
\end{aligned} \tag{A.2}$$

The combinations of quartic interactions λ_1 , λ_2 , and $\lambda_3 + \lambda_4$, appearing in the Hhh coupling may be written in terms of the physical masses m_h, m_H, m_A , the expectation value v , the mixing angles α and β , and the quartic interactions λ_5 , λ_6 , and λ_7 [36]

$$\lambda_1 = \frac{m_H^2 \cos^2 \alpha + m_h^2 \sin^2 \alpha - m_A^2 \sin^2 \beta}{v^2 \cos^2 \beta} - \lambda_5 \tan^2 \beta - 2\lambda_6 \tan \beta \tag{A.3}$$

$$\lambda_2 = \frac{m_H^2 \sin^2 \alpha + m_h^2 \cos^2 \alpha - m_A^2 \cos^2 \beta}{v^2 \sin^2 \beta} - \lambda_5 \cot^2 \beta - 2\lambda_7 \cot \beta \tag{A.4}$$

$$\lambda_3 + \lambda_4 = \frac{(m_H^2 - m_h^2) \sin \alpha \cos \alpha}{v^2 \sin \beta \cos \beta} + \frac{m_A^2}{v^2} - \lambda_6 \cot \beta - \lambda_7 \tan \beta \tag{A.5}$$

With these relations, the Hhh coupling for the tree-level potential (A.2) may be written

$$\begin{aligned}
g_{Hhh} = & \frac{\cos(\beta - \alpha)}{v} \left[(3m_A^2 + 3\lambda_5 v^2 - 2m_h^2 - m_H^2) \left(\cos(2\beta - 2\alpha) - \frac{\sin(2\beta - 2\alpha)}{\tan(2\beta)} \right) \right. \\
& - m_A^2 - \lambda_5 v^2 + \frac{\lambda_6 v^2}{2} (-\cot \beta + 3 \sin(2\beta - 2\alpha) + 3 \cot \beta \cos(2\beta - 2\alpha)) \\
& \left. + \frac{\lambda_7 v^2}{2} (-\tan \beta - 3 \sin(2\beta - 2\alpha) + 3 \tan \beta \cos(2\beta - 2\alpha)) \right]
\end{aligned} \tag{A.6}$$

The Hhh self coupling is homogenous in $\cos(\beta - \alpha)$, and vanishes in the alignment limit. Near the alignment limit it may be expanded in a power series about $\cos(\beta - \alpha) = 0$, with the result

$$\begin{aligned}
g_{Hhh} \simeq & -\frac{\cos(\beta - \alpha)}{v} \left[4m_A^2 - 2m_h^2 - m_H^2 + 4\lambda_5 v^2 \right. \\
& \left. + \frac{2v^2}{\tan(2\beta)} (\lambda_6 - \lambda_7) + \frac{2v^2}{\sin(2\beta)} (\lambda_6 + \lambda_7) + \mathcal{O}(\cos(\beta - \alpha)) \right]
\end{aligned} \tag{A.7}$$

The general expression (A.6) for the Hhh coupling simplifies in certain models. In the MSSM $\lambda_5 = \lambda_6 = \lambda_7 = 0$. In this case the Hhh coupling reduces to a function of the physical masses m_h, m_H, m_A and the mixing angles α and β

$$g_{Hhh}^{\text{MSSM}} = \frac{\cos(\beta - \alpha)}{v} \left[(3m_A^2 - 2m_h^2 - m_H^2) \left(\cos(2\beta - 2\alpha) - \frac{\sin(2\beta - 2\alpha)}{\tan(2\beta)} \right) - m_A^2 \right] \quad (\text{A.8})$$

This expression may be simplified using the the tree-level MSSM Higgs mass sum rule $m_h^2 + m_H^2 = m_Z^2 + m_A^2$, as well as the MSSM tree-level relations $m_A^2 = m_Z^2 \sin(2\alpha + 2\beta) / \sin(2\alpha - 2\beta)$ and $m_h^2 = m_Z^2 \cos(2\beta) \sin(\alpha + \beta) / \sin(\alpha - \beta)$, with the result

$$g_{Hhh}^{\text{MSSM}} = -\frac{m_Z^2}{v} \left[2 \sin(2\alpha) \sin(\beta + \alpha) - \cos(2\alpha) \cos(\beta + \alpha) \right] \quad (\text{A.9})$$

As another limit, 2HDMs with a Z_2 exchange symmetry $\Phi_1 \leftrightarrow \Phi_2$ have $m_{12}^2 = 0$ and $\lambda_6 = \lambda_7 = 0$. In this case $m_A^2 = -\lambda_5 v^2$, and the Hhh couplings reduces to a function of the masses m_h and m_H and the mixing angles α and β

$$g_{Hhh}^{Z_2} = -\frac{\cos(\beta - \alpha)}{v} \left[(2m_h^2 + m_H^2) \left(\cos(2\beta - 2\alpha) - \frac{\sin(2\beta - 2\alpha)}{\tan(2\beta)} \right) \right] \quad (\text{A.10})$$

This form of the Hhh coupling was used in a previous study of multi-lepton signatures of 2HDMs [4].

B Standard-Model Like Higgs Fit Data

For reference we collect here the data that is used in constructing fits of the SM-like Higgs couplings. In Tables 4, 5, 6 we show results from ATLAS, CMS, and the Tevatron respectively.

Channel	$\hat{\mu}$ (7 TeV)	$\zeta_i^{(G,V,T)}$ (%)	$\hat{\mu}$ (8 TeV)	$\zeta_i^{(G,V,T)}$ (%)	Refs.
$b\bar{b}$	comb. w/8	—	-0.42 ± 1.05	(0, 100, 0)	[65, 66]
$b\bar{b} (ttH)$	3.81 ± 5.78	(0, 30, 70)	—	—	
$\tau\tau$	comb. w/8	—	0.7 ± 0.7	(20, 80, 0)	[67]
$WW (0j)$	0.06 ± 0.60	inclusive	$0.92^{+0.63}_{-0.49}$	inclusive	
$WW (1j)$	$2.04^{+1.88}_{-1.30}$	inclusive	$1.11^{+1.20}_{-0.82}$	inclusive	[68]
$WW (2j)$	—	—	$1.79^{+0.94}_{-0.75}$	(20, 80, 0)	
ZZ	comb. w/8	—	$1.7^{+0.5}_{-0.4}$	inclusive	[69]
$\gamma\gamma_{(L)} (uc ct)$	$0.53^{+1.37}_{-1.44}$	(93, 7, 0)	0.86 ± 0.67	(93.7, 6.2, 0.2)	
$\gamma\gamma_{(H)} (uc ct)$	$0.17^{+1.94}_{-1.91}$	(67, 31, 2)	$0.92^{+1.1}_{-0.89}$	(79.3, 19.2, 1.4)	
$\gamma\gamma_{(L)} (uc ec)$	$2.51^{+1.66}_{-1.69}$	(93, 7, 0)	$2.51^{+0.84}_{-0.75}$	(93.2, 6.6, 0.1)	
$\gamma\gamma_{(H)} (uc ec)$	$10.39^{+3.67}_{-3.67}$	(65, 33, 2)	$2.69^{+1.31}_{-1.08}$	(78.1, 20.8, 1.1)	
$\gamma\gamma_{(L)} (c ct)$	$6.08^{+2.59}_{-2.63}$	(93, 7, 0)	$1.37^{+1.02}_{-0.88}$	(93.6, 6.2, 0.2)	
$\gamma\gamma_{(H)} (c ct)$	$-4.40^{+1.80}_{-1.76}$	(67, 31, 2)	$1.99^{+1.50}_{-1.22}$	(78.9, 19.6, 1.5)	
$\gamma\gamma_{(L)} (c ec)$	$2.73^{+1.91}_{-2.02}$	(93, 7, 0)	$2.21^{+1.13}_{-0.95}$	(93.2, 6.7, 0.1)	
$\gamma\gamma_{(H)} (c ec)$	$-1.63^{+2.88}_{-2.88}$	(65, 33, 2)	$1.26^{+1.31}_{-1.22}$	(77.7, 21.2, 1.1)	[53, 70]
$\gamma\gamma (c trans.)$	$0.35^{+3.56}_{-3.60}$	(89, 11, 0)	$2.80^{+1.64}_{-1.55}$	(90.7, 9.0, 0.2)	
$\gamma\gamma (dijet)$	$2.69^{+1.87}_{-1.84}$	(23, 77, 0)	—	—	
$\gamma\gamma (loose\ high\ mass\ jj)$	—	—	$2.76^{+1.73}_{-1.35}$	(45, 54.9, 0.1)	
$\gamma\gamma (tight\ high\ mass\ jj)$	—	—	$1.59^{+0.84}_{-0.62}$	(23.8, 76.2, 0)	
$\gamma\gamma (low\ mass\ jj)$	—	—	$0.33^{+1.68}_{-1.46}$	(48.1, 49.9, 1.9)	
$\gamma\gamma (E_T^{miss}\ significance)$	—	—	$2.98^{+2.70}_{-2.15}$	(4.1, 83.8, 12.1)	
$\gamma\gamma (lepton\ tag)$	—	—	$2.69^{+1.95}_{-1.66}$	(2.2, 79.2, 18.6)	

Table 4. Light Higgs fit data from ATLAS. We denote best fits on signal strength modifier as $\hat{\mu}$ and quote efficiencies ζ for production initiated by gluons (G), weak gauge bosons (V), and top quarks (T). For diphoton channels, ‘uc’ (‘c’) corresponds to unconverted (converted) photons, ‘ct’ indicates central photons, ‘ec’ indicates one or more photon in the endcap, and subscripts (H, L) designate high and low p_T .

References

- [1] **ATLAS Collaboration** Collaboration, G. Aad *et al.*, *Observation of a new particle in the search for the Standard Model Higgs boson with the ATLAS detector at the LHC*, *Phys.Lett. B* **716** (2012) 1–29, [[1207.7214](#)].
- [2] **CMS Collaboration** Collaboration, S. Chatrchyan *et al.*, *Observation of a new boson at a mass of 125 GeV with the CMS experiment at the LHC*, *Phys.Lett. B* **716** (2012) 30–61, [[1207.7235](#)].
- [3] N. Craig and S. Thomas, *Exclusive Signals of an Extended Higgs Sector*, *JHEP* **1211** (2012) 083, [[1207.4835](#)].
- [4] N. Craig, J. A. Evans, R. Gray, C. Kilic, M. Park, *et al.*, *Multi-Lepton Signals of Multiple Higgs Bosons*, **1210.0559**.
- [5] T. Lee, *A Theory of Spontaneous T Violation*, *Phys.Rev.* **D8** (1973) 1226–1239.
- [6] T. Lee, *CP Nonconservation and Spontaneous Symmetry Breaking*, *Phys.Rept.* **9** (1974)

Channel	$\hat{\mu}$ (7 TeV)	$\zeta_i^{(G,V,T)}$ (%)	$\hat{\mu}$ (8 TeV)	$\zeta_i^{(G,V,T)}$ (%)	Refs.
$b\bar{b}$	comb. w/8	—	$1.30^{+0.68}_{-0.59}$	(0, 100, 0)	[71]
$b\bar{b}$ (ttH)	$-0.81^{+2.05}_{-1.75}$	(0, 30, 70)	—	—	[72]
$\tau\tau$ (0/1j)	comb. w/8	—	$0.74^{+0.49}_{-0.52}$	inclusive	[73]
$\tau\tau$ (VBF)	comb. w/8	—	$1.38^{+0.61}_{-0.57}$	(0, 100, 0)	
$\tau\tau$ (VH)	comb. w/8	—	$0.76^{+1.48}_{-1.43}$	(0, 100, 0)	
WW (0/1j)	comb. w/8	—	0.76 ± 0.21	inclusive	[74]
WW (2j)	comb. w/8	—	$-0.05^{+0.73}_{-0.56}$	(17, 83, 0)	
WW (VH)	comb. w/8	—	$-0.31^{+2.24}_{-1.96}$	(0, 100, 0)	
ZZ (untagged)	comb. w/8	—	$0.84^{+0.32}_{-0.26}$	(95, 5, 0)	[75]
ZZ (dijet tag)	—	—	$1.22^{+0.84}_{-0.57}$	(80, 20, 0)	
$\gamma\gamma$ (untagged 0)	$3.78^{+2.01}_{-1.62}$	(61.4, 35.5, 3.1)	$2.12^{+0.92}_{-0.78}$	(72.9, 24.6, 2.6)	[76]
$\gamma\gamma$ (untagged 1)	$0.15^{+0.99}_{-0.92}$	(87.6, 11.8, 0.5)	$-0.03^{+0.71}_{-0.64}$	(83.5, 15.5, 1.0)	
$\gamma\gamma$ (untagged 2)	-0.05 ± 1.21	(91.3, 8.3, 0.3)	$0.22^{+0.46}_{-0.42}$	(91.7, 7.9, 0.4)	
$\gamma\gamma$ (untagged 3)	$1.38^{+1.66}_{-1.55}$	(91.3, 8.5, 0.2)	$-0.81^{+0.85}_{-0.42}$	(92.5, 7.2, 0.2)	
$\gamma\gamma$ (dijet)	$4.13^{+2.33}_{-1.76}$	(26.8, 73.1, 0.0)	—	—	
$\gamma\gamma$ (dijet loose)	—	—	$0.75^{+1.06}_{-0.99}$	(46.8, 52.8, 0.5)	
$\gamma\gamma$ (dijet tight)	—	—	$0.22^{+0.71}_{-0.57}$	(20.7, 79.2, 0.1)	
$\gamma\gamma$ (MET)	—	—	$1.84^{+2.65}_{-2.26}$	(0.0, 79.3, 20.8)	
$\gamma\gamma$ (Electron)	—	—	$-0.70^{+2.75}_{-1.94}$	(1.1, 79.3, 19.7)	
$\gamma\gamma$ (Muon)	—	—	$0.36^{+1.84}_{-1.38}$	(21.1, 67.0, 11.8)	

Table 5. Light Higgs fit data from CMS.

Exp.	Channel	$\hat{\mu}$ (2 TeV)	$\zeta^{(G,V,T)}$ (%)	Ref.
CDF	$b\bar{b}$	$1.72^{+0.92}_{-0.87}$	(0, 100, 0)	[77, 78]
	$\tau\tau$	$0.00^{+8.44}_{-0.00}$	(50, 50, 0)	
	WW	$0.00^{+1.78}_{-0.00}$	inclusive	
	$\gamma\gamma$	$7.81^{+4.61}_{-4.42}$	inclusive	
DØ	$b\bar{b}$	$1.23^{+1.24}_{-1.17}$	(0, 100, 0)	[77, 78]
	$\tau\tau$	$3.94^{+4.11}_{-4.38}$	(50, 50, 0)	
	WW	$1.90^{+1.63}_{-1.52}$	inclusive	
	$\gamma\gamma$	$4.20^{+4.60}_{-4.20}$	inclusive	

Table 6. Light Higgs fit data from CDF/DØ. Production efficiencies in $\tau\tau$ channels are approximated from [79].

143–177.

- [7] P. Fayet, *A Gauge Theory of Weak and Electromagnetic Interactions with Spontaneous Parity Breaking*, *Nucl.Phys.* **B78** (1974) 14.
- [8] R. A. Flores and M. Sher, *Higgs Masses in the Standard, Multi-Higgs and Supersymmetric Models*, *Annals Phys.* **148** (1983) 95.
- [9] S. Dimopoulos and H. Georgi, *Softly Broken Supersymmetry and SU(5)*, *Nucl.Phys.* **B193** (1981) 150.

- [10] Z. Chacko, Y. Nomura, M. Papucci, and G. Perez, *Natural little hierarchy from a partially goldstone twin Higgs*, *JHEP* **0601**, 126 (2006), [[hep-ph/0510273](#)].
- [11] J. Mrazek, A. Pomarol, R. Rattazzi, M. Redi, J. Serra, *et al.*, *The Other Natural Two Higgs Doublet Model*, *Nucl.Phys.* **B853** (2011) 1–48, [[1105.5403](#)].
- [12] J. Gunion and H. E. Haber, *Higgs Bosons in Supersymmetric Models. 2. Implications for Phenomenology*, *Nucl.Phys.* **B278** (1986) 449.
- [13] M. Spira, A. Djouadi, D. Graudenz, and P. Zerwas, *SUSY Higgs production at proton colliders*, *Phys.Lett.* **B318** (1993) 347–353.
- [14] M. S. Carena, S. Mrenna, and C. Wagner, *MSSM Higgs boson phenomenology at the Tevatron collider*, *Phys.Rev.* **D60** (1999) 075010, [[hep-ph/9808312](#)].
- [15] M. S. Carena, S. Mrenna, and C. Wagner, *The Complementarity of LEP, the Tevatron and the CERN LHC in the search for a light MSSM Higgs boson*, *Phys.Rev.* **D62** (2000) 055008, [[hep-ph/9907422](#)].
- [16] M. Carena, E. Ponton, and J. Zurita, *BMSSM Higgs Bosons at the 7 TeV LHC*, *Phys.Rev.* **D85** (2012) 035007, [[1111.2049](#)].
- [17] S. Chang, J. A. Evans, and M. A. Luty, *Possibility of early Higgs boson discovery in nonminimal Higgs sectors*, *Phys.Rev.* **D84** (2011) 095030, [[1107.2398](#)].
- [18] J. F. Gunion, H. E. Haber, G. L. Kane, and S. Dawson, *THE HIGGS HUNTER'S GUIDE*, *Front.Phys.* **80** (2000) 1–448.
- [19] G. Branco, P. Ferreira, L. Lavoura, M. Rebelo, M. Sher, *et al.*, *Theory and phenomenology of two-Higgs-doublet models*, *Phys.Rept.* **516** (2012) 1–102, [[1106.0034](#)].
- [20] P. Ferreira, R. Santos, M. Sher, and J. P. Silva, *Implications of the LHC two-photon signal for two-Higgs-doublet models*, *Phys.Rev.* **D85** (2012) 077703, [[1112.3277](#)].
- [21] P. Ferreira, R. Santos, M. Sher, and J. P. Silva, *Could the LHC two-photon signal correspond to the heavier scalar in two-Higgs-doublet models?*, *Phys.Rev.* **D85** (2012) 035020, [[1201.0019](#)].
- [22] D. S. Alves, P. J. Fox, and N. J. Weiner, *Higgs Signals in a Type I 2HDM or with a Sister Higgs*, [1207.5499](#).
- [23] G. Belanger, U. Ellwanger, J. Gunion, Y. Jiang, and S. Kraml, *Two Higgs Bosons at the Tevatron and the LHC?*, [1208.4952](#).
- [24] W. Altmannshofer, S. Gori, and G. D. Kribs, *A Minimal Flavor Violating 2HDM at the LHC*, *Phys.Rev.* **D86** (2012) 115009, [[1210.2465](#)].
- [25] Y. Bai, V. Barger, L. L. Everett, and G. Shaughnessy, *The 2HDM-X and Large Hadron Collider Data*, [1210.4922](#).
- [26] A. Drozd, B. Grzadkowski, J. F. Gunion, and Y. Jiang, *Two-Higgs-Doublet Models and Enhanced Rates for a 125 GeV Higgs*, [1211.3580](#).
- [27] J. Chang, K. Cheung, P.-Y. Tseng, and T.-C. Yuan, *Implications on the Heavy CP-even Higgs Boson from Current Higgs Data*, *Phys. Rev. D* **87**, **035008** (2003) [[1211.3849](#)].
- [28] J. Chang, K. Cheung, P.-Y. Tseng, and T.-C. Yuan, *Various Models Mimicking the SM Higgs Boson*, *Int.J.Mod.Phys.* **A27** (2012) 1230030, [[1211.6823](#)].

- [29] G. Belanger, B. Dumont, U. Ellwanger, J. Gunion, and S. Kraml, *Higgs Couplings at the End of 2012*, *JHEP* **1302** (2013) 053, [[1212.5244](#)].
- [30] C.-Y. Chen and S. Dawson, *Exploring Two Higgs Doublet Models Through Higgs Production*, [1301.0309](#).
- [31] A. Celis, V. Ilisie, and A. Pich, *LHC constraints on two-Higgs doublet models*, [1302.4022](#).
- [32] C.-W. Chiang and K. Yagyu, *Implications of Higgs boson search data on the two-Higgs doublet models with a softly broken Z_2 symmetry*, [1303.0168](#).
- [33] B. Grinstein and P. Uttayarat, *Carving Out Parameter Space in Type-II Two Higgs Doublets Model*, [1304.0028](#).
- [34] A. Azatov, R. Contino, and J. Galloway, *Model-Independent Bounds on a Light Higgs*, *JHEP* **1204** (2012) 127, [[1202.3415](#)].
- [35] S. L. Glashow and S. Weinberg, *Natural Conservation Laws for Neutral Currents*, *Phys.Rev.* **D15** (1977) 1958.
- [36] J. F. Gunion and H. E. Haber, *The CP conserving two Higgs doublet model: The Approach to the decoupling limit*, *Phys.Rev.* **D67** (2003) 075019, [[hep-ph/0207010](#)].
- [37] D. Carmi, A. Falkowski, E. Kuflik, and T. Volansky, *Interpreting LHC Higgs Results from Natural New Physics Perspective*, *JHEP* **1207** (2012) 136, [[1202.3144](#)].
- [38] J. Espinosa, C. Grojean, M. Muhlleitner, and M. Trott, *Fingerprinting Higgs Suspects at the LHC*, *JHEP* **1205** (2012) 097, [[1202.3697](#)].
- [39] T. Li, X. Wan, Y.-k. Wang, and S.-h. Zhu, *Constraints on the Universal Varying Yukawa Couplings: from SM-like to Fermiophobic*, *JHEP* **1209** (2012) 086, [[1203.5083](#)].
- [40] J. Ellis and T. You, *Global Analysis of Experimental Constraints on a Possible Higgs-Like Particle with Mass ~ 125 GeV*, *JHEP* **1206** (2012) 140, [[1204.0464](#)].
- [41] A. Azatov, R. Contino, D. Del Re, J. Galloway, M. Grassi, *et al.*, *Determining Higgs couplings with a model-independent analysis of h to $\gamma\gamma$* , *JHEP* **1206** (2012) 134, [[1204.4817](#)].
- [42] M. Klute, R. Lafaye, T. Plehn, M. Rauch, and D. Zerwas, *Measuring Higgs Couplings from LHC Data*, *Phys.Rev.Lett.* **109** (2012) 101801, [[1205.2699](#)].
- [43] A. Azatov, S. Chang, N. Craig, and J. Galloway, *Higgs fits preference for suppressed down-type couplings: Implications for supersymmetry*, *Phys.Rev.* **D86** (2012) 075033, [[1206.1058](#)].
- [44] I. Low, J. Lykken, and G. Shaughnessy, *Have We Observed the Higgs (Imposter)?*, *Phys.Rev.* **D86** (2012) 093012, [[1207.1093](#)].
- [45] T. Corbett, O. Eboli, J. Gonzalez-Fraile, and M. Gonzalez-Garcia, *Constraining anomalous Higgs interactions*, *Phys.Rev.* **D86** (2012) 075013, [[1207.1344](#)].
- [46] M. Montull and F. Riva, *Higgs discovery: the beginning or the end of natural EWSB?*, *JHEP* **1211** (2012) 018, [[1207.1716](#)].
- [47] J. Espinosa, C. Grojean, M. Muhlleitner, and M. Trott, *First Glimpses at Higgs' face*, *JHEP* **1212** (2012) 045, [[1207.1717](#)].
- [48] D. Carmi, A. Falkowski, E. Kuflik, T. Volansky, and J. Zupan, *Higgs After the Discovery: A Status Report*, *JHEP* **1210** (2012) 196, [[1207.1718](#)].

- [49] P. P. Giardino, K. Kannike, I. Masina, M. Raidal, and A. Strumia, *The universal Higgs fit*, [1303.3570](#).
- [50] J. Ellis and T. You, *Updated Global Analysis of Higgs Couplings*, [1303.3879](#).
- [51] A. Djouadi and G. Moreau, *The couplings of the Higgs boson and its CP properties from fits of the signal strengths and their ratios at the 7+8 TeV LHC*, [1303.6591](#).
- [52] A. Azatov and J. Galloway, *Electroweak Symmetry Breaking and the Higgs Boson: Confronting Theories at Colliders*, *Int.J.Mod.Phys.* **A28** (2013) 1330004, [[1212.1380](#)].
- [53] G. Aad *et al.* [ATLAS Collaboration], *Search for the Standard Model Higgs boson in the diphoton decay channel with 4.9 fb^{-1} of pp collisions at $\sqrt{s} = 7 \text{ TeV}$ with ATLAS*, *Phys. Rev. Lett.* **108**, 111803 (2012) [[1202.1414](#)].
- [54] **LHC Higgs Cross Section Working Group** Collaboration, S. Dittmaier *et al.*, *Handbook of LHC Higgs Cross Sections: 1. Inclusive Observables*, [1101.0593](#).
- [55] R. V. Harlander and W. B. Kilgore, *Higgs boson production in bottom quark fusion at next-to-next-to leading order*, *Phys.Rev.* **D68** (2003) 013001, [[hep-ph/0304035](#)].
- [56] A. Djouadi, M. Spira, and P. M. Zerwas, *QCD corrections to hadronic Higgs decays*, *Z. Phys.* **C70**, 427 (1996), [[hep-ph/9511344](#)].
- [57] A. Djouadi, *The Anatomy of electro-weak symmetry breaking. II. The Higgs bosons in the minimal supersymmetric model*, *Phys. Rept.* **459**, 1 (2008), [[hep-ph/0503173](#)].
- [58] A. Djouadi, J. Kalinowski, and P. Zerwas, *Two and three-body decay modes of SUSY Higgs particles*, *Z.Phys.* **C70** (1996) 435–448, [[hep-ph/9511342](#)].
- [59] M. Sher, *Review of prospects for H^+ in non-SUSY multi-Higgs models in view of LHC results*, [1212.0789](#).
- [60] S. Chatrchyan *et al.* [CMS Collaboration], *Search for a standard-model-like Higgs boson with a mass of up to 1 TeV at the LHC*, [[1304.0213](#)].
- [61] J. F. Gunion, Y. Jiang, and S. Kraml, *Diagnosing Degenerate Higgs Bosons at 125 GeV*, *Phys. Rev. Lett.* **110**, 051801 (2013), [[1208.1817](#)].
- [62] A. Djouadi and J. Quevillon, *The MSSM Higgs sector at a high M_{SUSY} : reopening the low $\tan\beta$ regime and the search for heavy Higgses*, [arXiv:1304.1787](#).
- [63] B. Coleppa, F. Kling, and S. Su, *Constraining Type II 2HDM in Light of LHC Higgs Searches*, [arXiv:1305.0002](#).
- [64] C. -Y. Chen, S. Dawson, and M. Sher, *Heavy Higgs Searches and Constraints on Two Higgs Doublet Models*, [arXiv:1305.1624](#).
- [65] ATLAS Collaboration, ATLAS-CONF-2012-161.
- [66] ATLAS Collaboration, ATLAS-CONF-2012-135.
- [67] G. Aad *et al.* [ATLAS Collaboration], *Search for the Standard Model Higgs boson in the H to $\tau^+\tau^-$ decay mode in $\sqrt{s} = 7 \text{ TeV}$ pp collisions with ATLAS*, *JHEP* **1209**, 070 (2012) [[1206.5971](#)]; ATLAS-CONF-2012-160.

- [68] G. Aad *et al.* [ATLAS Collaboration], *Search for the Standard Model Higgs boson in the $H \rightarrow WW^{(*)} \rightarrow \ell\nu\ell\nu$ decay mode with 4.7 /fb of ATLAS data at $\sqrt{s} = 7$ TeV* Phys. Lett. B **716**, 62 (2012) [[1206.0756](#)]; ATLAS-CONF-2013-030.
- [69] G. Aad *et al.* [ATLAS Collaboration], *Search for the Standard Model Higgs boson in the decay channel $H \rightarrow ZZ^{(*)} \rightarrow 4\ell$ with 4.8 fb-1 of pp collision data at $\sqrt{s} = 7$ TeV with ATLAS*, Phys. Lett. B **710**, 383 (2012) [[1202.1415](#)]; ATLAS-CONF-2013-013.
- [70] ATLAS Collaboration, ATLAS-CONF-2013-012.
- [71] S. Chatrchyan *et al.* [CMS Collaboration], *Search for the standard model Higgs boson decaying to bottom quarks in pp collisions at $\sqrt{s}=7$ TeV*, Phys. Lett. B **710**, 284 (2012) [[1202.4195](#)].
- [72] CMS Collaboration, CMS-PAS-HIG-12-025.
- [73] CMS Collaboration, CMS-PAS-HIG-12-043; CMS-PAS-HIG-13-004.
- [74] CMS Collaboration, CMS-HIG-12-042; CMS-HIG-13-003; CMS-HIG-13-009.
- [75] CMS Collaboration, CMS-HIG-12-023; CMS-HIG-13-002.
- [76] CMS Collaboration, CMS-PAS-HIG-12-015; CMS-PAS-HIG-13-001.
- [77] C. a. D. C. a. t. T. N. P. a. H. W. Group [Tevatron New Physics Higgs Working Group and CDF and D0 Collaborations], *Updated Combination of CDF and D0 Searches for Standard Model Higgs Boson Production with up to 10.0 fb⁻¹ of Data*, [[1207.0449](#)].
- [78] See talks from L. Zivkovic and W.-M. Yao at “Rencontres de Moriond”, March 2013: [<https://indico.in2p3.fr/conferenceOtherViews.py?view=standard&confId=7411>].
- [79] V. M. Abazov *et al.* [D0 Collaboration], *Search for the Higgs boson in lepton, tau and jets final states*, [[1211.6993](#)].